

REPORT DOCUMENT

Form Approved
OMB No 0704-01881a. REPORT SECURITY CLASSIFICATION
unclassified

2a. SECURITY CLASSIFICATION AUTHORITY

2b. DECLASSIFICATION/DOWNGRADING SCHEDULE

4. PERFORMING ORGANIZATION REPORT NUMBER(S)

6a. NAME OF PERFORMING ORGANIZATION

R & D Associates, Inc.

6c. ADDRESS (City, State, and ZIP Code)

301 S. West St.
Alexandria, VA 223148a. NAME OF FUNDING/SPONSORING
ORGANIZATION

AFOSR/NA

8c. ADDRESS (City, State, and ZIP Code)

Building 410, Bolling AFB, DC
20332-6448

11. TITLE (Include Security Classification)

(U) MPD Thrust Chamber Flow Dynamics

12. PERSONAL AUTHOR(S)

13a. TYPE OF REPORT

Final

13b. TIME COVERED

FROM 1 Oct 88 TO 30 Oct 89

14. DATE OF REPORT (Year, Month, Day)

90-08-23

15. PAGE COUNT

42

16. SUPPLEMENTARY NOTATION

17. COSATI CODES

FIELD GROUP SUB-GROUP

18. SUBJECT TERMS (Continue on reverse if necessary and identify by block number)

Electric propulsion, magnetoplasdynamic, arcjet

19. ABSTRACT (Continue on reverse if necessary and identify by block number)

Flow within the thrust chamber of an MPD arcjet is examined experimentally and modeled with a two-dimensional MHD code. Two quasi-steady MPD thrusters are considered under the same input conditions of current (21 kA) and total mass flow rate (6×10^{-3} kg/s, argon + 1.5% hydrogen). The arcjets have the same basic design, consisting of a central cathode, 3.8 cm diameter and 5 cm long, separated from a coaxial anode of equal length by a uniform gap of 2.3 cm. Two different mass injection arrangements are used (100% at mid-radius, and 50% at the cathode base, with the remainder at mid-radius). A new spectroscopic analysis procedure is developed that allows distributions of radial speed, heavy-particle temperature and turbulent speed to be extracted from chordal measurements of light emission by the two species in the plasma flow. Good qualitative

20. DISTRIBUTION/AVAILABILITY OF ABSTRACT

☒ UNCLASSIFIED/UNLIMITED ☒ SAME AS RPT.☒ DTIC USERS

21. ABSTRACT SECURITY CLASSIFICATION

Unclassified

22a. NAME OF RESPONSIBLE INDIVIDUAL

Dr. Mitat Birkan

22b. TELEPHONE (Include Area Code)

(202) 767-4937

22c. OFFICE SYMBOL

AFOSR/NA

(u)

19. cont.

(and reasonable quantitative) agreement exists with distributions calculated by the MHD code, indicating that flow within the thrust chamber expands from an electromagnetically-pumped plasma base (vs a pumped jet off the cathode tip). The significant variation of internal flow dynamics with mass injector arrangement implies the need for extensive experimentally-validated code modeling in order to evaluate the potential performance of MPD thrusters.

RDA-TR-144200-003

AFOSR-TR- 90 09 26

MPD THRUST CHAMBER FLOW DYNAMICS

Final Technical Report

August 1990

Prepared for:

**DEPARTMENT OF THE AIR FORCE
AIR FORCE OFFICE OF SCIENTIFIC RESEARCH
BOLLING AIR FORCE BASE, DC 20332-6448**

Prepared by:

RDA/WRL Staff

**R & D ASSOCIATES, WASHINGTON RESEARCH LABORATORY
301A S. WEST STREET, ALEXANDRIA, VIRGINIA 22314**

TELEPHONE 703 684-0333

RDA

Re: Arcjet
 F49620-86-C-0017
 Arcjet
 JFMA
 7/14/90

23 August 1990

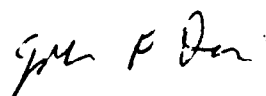
Department of the Air Force
 Air Force Office of Scientific Research
 ATTN: Dr. Mitat Birkan
 Building 410
 Bolling Air Force Base, DC 20332-6448

SUBJECT: Contract F49620-86-C-0017
 MPD Arcjet Thrust Chamber Flow Dynamics

Dear Dr. Birkan:

Enclosed are six copies of the Final Technical Report "MPD Arcjet Thrust Chamber Flow Dynamics" in accordance with the requirements of Contract F49620-86-C-0017, Research Item 0001AC, Option 2 and Item 0002AA". Please refer any technical questions to me at (703) 684-0333.

Sincerely,



John F. Davis
 Research Scientist

JFD
 Enclosures (as noted)
 cc: Mr. H. Haraldsen (PKD)

Accession For	
NTIS GRA&I	<input checked="" type="checkbox"/>
DTIC TAB	<input type="checkbox"/>
Unannounced	<input type="checkbox"/>
Justification	
By	
Distribution	
Availability Codes	
Dist	Availability Codes
A-1	

FINAL TECHNICAL REPORT

For the period 1 October 88 to 30 October 1989

MPD THRUST CHAMBER FLOW DYNAMICS

Prepared for:

DEPARTMENT OF THE AIR FORCE
AIR FORCE OFFICE OF SCIENTIFIC RESEARCH
BOLLING AIR FORCE BASE, DC 20332-6448

Prepared by:

RDA/WRL Staff

TABLE OF CONTENTS

LIST OF ILLUSTRATIONS

I. SUMMARY	1
II. INTRODUCTION	2
III. EXPERIMENTAL APPARATUS	3
IV. EXPERIMENTAL RESULTS	5
V. MHD CODE RESULTS	12
VI. CONCLUSIONS	13
VII. REFERENCES	15
VIII. APPENDIX	27

MPD ARCJET THRUST CHAMBER FLOW STUDIES

LIST OF ILLUSTRATIONS	PAGE
1. Schematic of MPD arcjet for study of MPD thrust chamber flow dynamics. Gas injection is through 16 choked orifices at mid-radius in boron nitride backplate.	17
2. MPD arcjet operating characteristics: a) current delivered to the MPD arcjet has a FWHM of 0.88 ms with a risetime of 0.1 ms. An initial charge of 8 kV on the LC-ladder capacitor bank gives a current of approximately 21 kA; b) terminal voltage at the arcjet (not corrected for inductive voltage transients) attains a quasi-equilibrium value about 0.2 ms after current initiation.	18
3. Basic layout of the MPD arcjet experiment. In the present experiments, the line of sight is actually through slits in the outer electrode of the thruster.	19
4. Current contours in the MPD arcjet operating at 21 kiloamps and 6×10^{-3} kg/s; a) for the case of mass injection only at mid-radius indicates that the current does not fill the thrust chamber and has radial force components towards the cathode center conductor, b) for the case of 50% mass injection near the cathode base and 50% at mid-radius indicates more than 20% of the current external to the thrust chamber with reduced radial force components.	20
5. Relative intensity of argon ion emission (integrated over the line profile) versus radial position from Abel inversion of Ar II 434.803 nm emission is peaked toward the cathode at 19.05 mm) and monotonically decreases.	21
6. Line profile of Ar II line at 13.6 mm from the cathode surface. Least-squares fit to a Gaussian profile is also shown.	21
7. Calculated electron density versus distance from the cathode from Lorentzian component of line profile fit to hydrogen 696.28 nm emission.	22
8. The emission profile versus wavelength from an axisymmetric flow from equivalent differential volume elements a y and y' will not be equal in the presence of radial velocity components. The emission profile at y' will be Doppler shifted to $\pm \lambda_0 V_r \sin \theta / c$ where λ_0 is the line center.	22
9. Application of new diagnostic technique in the study of the internal flow dynamics of an MPD arcjet with a cathode center conductor and inner electrode spacing of 2.3 cm for the case of mid-radius only mass injection shows radial velocities on the order of 10 km/s.	23
10. Distribution of gas temperature (upper curve) and turbulent speed (lower curve) for the case of mid-radius only mass injection, based on both argon and hydrogen emission analysis.	23

11. Application of new diagnostic technique in the study of the internal flow dynamics of an MPD arcjet with a cathode center conductor and inner electrode spacing of 2.3 cm for the case of 50% mass injection at cathode base and 50% at mid-radius shows radial velocities on the order of 3 km/s. 24
12. Distribution of gas temperature (upper curve) and turbulent speed (lower curve) for the case of 50% mass injection at cathode base, based on both argon and hydrogen emission analysis indicates reduced turbulent speeds to less than 1 km/s. 24
13. Current contours calculated by MACH2 computer code for case of uniform mass injection (at 6 g/s) through insulator backplate. Total current in 21 kA. 25
14. Constant temperature contours in units of (eV) calculated by MACH2 computer code for case of Fig. 13. 25
15. Constant atom number density contours in units of (cm^{-3}) calculated by MACH2 computer code for case of Fig. 13. 26
16. Distribution of flow velocity calculated by MACH2 computer code for case of Fig. 13. Magnitude of longest vector (well downstream of cathode corner) is 3.5×10^4 m/s. 26

I. SUMMARY

Flow within the thrust chamber of an MPD arcjet is examined experimentally and modeled with a two-dimensional MHD code. Two quasi-steady MPD thrusters are considered under the same input conditions of current (21 kA) and total mass flow rate (6×10^{-3} kg/s, argon + 1.5% hydrogen). The arcjets have the same basic design, consisting of a central cathode, 3.8 cm diameter and 5 cm long, separated from a coaxial anode of equal length by a uniform gap of 2.3 cm. Two different mass injection arrangements are used (100% at mid-radius, and 50% at the cathode base, with the remainder at mid-radius). A new spectroscopic analysis procedure is developed that allows distributions of radial speed, heavy-particle temperature and turbulent speed to be extracted from chordal measurements of light emission by the two species in the plasma flow. Good qualitative (and reasonable quantitative) agreement exists with distributions calculated by the MHD code, indicating that flow within the thrust chamber expands from an electromagnetically-pumped plasma base (vs a pumped jet off the cathode tip). The significant variation of internal flow dynamics with mass injector arrangement implies the need for extensive experimentally-validated code modeling in order to evaluate the potential performance of MPD thrusters.

II. INTRODUCTION

For the last twenty-five years, there has been continued interest in the so-called magnetoplasmadynamic (MPD) arcjet. Operation of an arcjet in the MPD mode was discovered by A. Ducati in the course of research on arcjet performance in which he lowered the input mass flow rate to the thrust chamber and found that a relatively benign discharge condition could be achieved.¹ Rather than leading to higher chamber temperatures with increased erosion of the electrodes the reduction in mass flow provided increased lifetime, higher specific impulse, and (for hydrogen, at least) higher efficiency. These improvements were accomplished in a device that retained the simplicity of conventional arcjets in regard to construction, parts-count, and power supply requirements. Subsequent studies extended operation to propellants other than hydrogen, and included various arrangements of auxiliary magnetic fields, and electrode geometries.²⁻⁶ MPD arcjet became a general appellation for devices ranging from steady conventional arcjets (operating at higher current and/or lower mass flow rate than thermal arcjets), pulsed high current discharges (descended from plasma-pinch engines), and cross-field Hall accelerator arrangements (e.g. see comments by Jahn in ref. 7). Along with the broadening of the MPD arcjet category (which at best might recognize a commonality of physical mechanisms or concerns) came a profusion of theoretical models and experimental data, which were often consistent within individual devices, but in conflict when applied across the entire class of thrusters. The difficulty of probing within the small (~ few mm) chamber dimensions of steady-state devices, and the need to identify thruster arrangements/regimes with attractive performance values has involved a concentration on terminal measurements, such as current, voltage, and thrust. Detailed diagnosis of the structure of the discharge and flow within the thrust chamber has been attempted only in the higher power (~ megawatt) quasi-steady laboratory devices, and even then, only for a limited range of operating conditions.⁸⁻¹⁴

The particular difficulties with understanding MPD arcjet performance in terms of the actual thrust and energy transfer mechanisms within the arcjet chamber have been twofold: an inability to monitor experimentally changes in flow structure with variation in terminal conditions; and inability to model accurately the two-dimensional,

electromagnetically-powered discharge flow. The present paper discusses recent progress in overcoming these difficulties in terms of a new spectroscopic technique for obtaining thrust chamber flow conditions, and the application of a two-dimensional MHD code developed originally for pulsed, coaxial plasma gun modeling.¹⁵

III. EXPERIMENTAL APPARATUS

A. Experimental Technique and Equipment

At the R&D Associates Washington Research Laboratory, the experimental facility for the study of MPD arcjets uses a 6 meter long stainless steel vacuum tank with a 0.61 m inside diameter. The tank has two coaxial 35.6 cm diameter diagnostic ports for an optically clear view through the test section. In addition, there is an electrical feed-through port and two 8-inch diffusion pump ports at opposite ends of the tank that are connected to two 2000 liters/sec diffusion pumps. The base vacuum of the system is of the order of 1.5×10^{-6} Torr.

Two MPD arcjet configurations have been used for the study of internal flow dynamics: 1) all orifices at the mid-radius of the chamber backplate as shown in Figure 1; and 2) half the mass flow through orifices at mid-radius, and the remainder through orifices opening to a circular groove surrounding the cathode base. The latter arrangement was prompted by the apparent deposition of cathode material on the boron nitride insulator after extended use of mid-radius-only injection. Both arcjet configurations has a brass outer anode with a copper-tungsten alloy cathode. The inner electrode gap is 23 mm and the channel length is 50 mm. Argon with 1.5% hydrogen mixtures were feed to the experiment via six optically triggered fast puff valves providing a quasi-steady mass flow into the thrust chamber through choked orifices in the boron nitride backplate. The fast puff valves had a rise time of approximately 4 msec to 90% peak flow with a flow duration as determined by the gas plenum (typically 8 msec). In both experimental arrangements, the total mass flow was 6×10^{-3} kg/s.

The discharge is powered by a 400 kJ capacitor bank connected as an LC-ladder network. At an initial voltage of 18 kV, approximately 45 kA can be delivered to the experiment with a full width at half maximum (FWHM) of 0.88 msec; a simple change in connection can provide ~90 kA with a FWHM of 0.44 msec. Voltage and current

measurements are recorded with digital data acquisition equipment and analyzed with a dedicated data analysis computer in an adjacent screen room.

B. Arcjet Operating Characteristics

Typical discharge current and terminal voltage (uncorrected for initial and final inductive transients) are displayed vs time in Figures 2a & 2b for a charge on the capacitor bank of 8 kV and a mass flow rate of 6×10^{-3} kg/s. Quasi-steady operation, as indicated by these measurements, is obtained after about 150 μ s and persists for about 550 μ s with a discharge current plateau of approximately 21 kA and a voltage of 48 V. The terminal voltage is monitored with a 1000:1 voltage probe with the signal to the screen room via a optical data link. The high frequency noise on the terminal voltage waveform is a consequence of the optical data link receiver and does not reflect voltage fluctuations at the arcjet.

The input power during the quasi-steady phase is therefore ~ 1 MW, which, reasonably corresponds to high power, quasi-steady MPD arcjet operation studied by other groups for many years.^{12,14} Based on such studies, plasma speeds on the order of 10^4 m/s are expected. Such speeds would provide Doppler shifts/widths, $\Delta\lambda/\lambda_0 = u/c \approx 3.3 \times 10^{-5}$, or $\Delta\lambda \approx 0.014$ nm (for the AR II line at 434.8 nm). For sufficient dispersion by a spectrograph, in combination with electronic amplification of the observed light intensity, non-intrusive measurement of heavy-particle speeds should be possible. Furthermore, it should be possible to sample entire sections of the arcjet flow field in a single test shot by employing a two-dimensional detector array.

C. Spectroscopic System

For spectroscopic analysis of the entire flow field, a digital spectral and spatial data acquisition system has been developed at the RDA Washington Research Laboratory in a cooperative program with a group at the Massachusetts Institute of Technology¹⁴. The system, displayed schematically in Figure 3, is comprised of a 1.2 meter, f/11.5 spectrograph with a EG&G/PARC silicon intensified optical multichannel analyzer (OMA-SIT camera). The OMA-SIT is a two-dimensional (500 x 500) sensor array that can be gated on and off with a pulse width down to 40 ns. The spectroscopic system with input optics is mounted on an optical bench adjacent to the experiment.

In order to make measurements within the arcjet thrust chamber, a series of four slits were machined symmetrically in the outer conductor 1.6mm wide at a position

22.7mm from the insulator. By aligning the spectrograph slit perpendicular to the axis of symmetry of the MPD accelerator simultaneous chordal views can be sampled through the slit in the outer conductor. This light is then dispersed spectrally onto the two-dimensional sensor array of the OMA-SIT camera thereby providing intensity information as a function of wavelength and position along the slit.

The spectral and spatial output from the camera is processed by an IBM System 9000 laboratory computer for immediate background subtraction and signal averaging. Each data acquisition in normal operation is comprised of 62.5 kbytes of wavelength versus position versus intensity data. Software permits the spectrum at any slit position (i.e. chordal position) to be displayed and manipulated. In particular, corrections for systematic errors and noise can be incorporated directly, prior to attempting analysis of line shape (at a given slit position) or intensity vs position (at a given wavelength). The present data collection configuration yields a wavelength resolution of 0.00113 nm/pixel in 3rd order at 434.8 nm with a spatial resolution at the experiment of 0.25 mm/pixel.

IV. EXPERIMENTAL RESULTS

A. Inter-electrode Current Distribution

In addition to the spectroscopic diagnostic systems, magnetic probes (integrating the local $\partial B/\partial t$) are used to delineate the discharge structure within the thrust chamber. Two magnetic probes were used made of 20 turns of thin Cu wire with an effective diameter of 1.2mm encased in sealed pyrex tubes 3mm diameter. The two magnetic probes were mounted on an xy-translator with external positioning and with a positioning accuracy of ~ 0.2 mm. Current contours developed over repeated test firings are displayed in Figures 4a and 4b for the two arrangements of mass injection, as indicated. Note that the current distribution for the case with mass flow through orifices at the mid-radius (Figure 4a) is basically retained within the arcjet thrust chamber, with less than 5% of the total current beyond the exit plane. There were also clear indications that near the boron nitride insulator the current distribution was perturbed in response to the entry of relatively high density, low speed flow through the gas inlet ports. With half the mass flow through orifices at mid-radius, and the remainder through an opening at the cathode base (Figure 4b), more than 20% of the total current is beyond the exit plane. In addition, less

radial $j \times B$ forces on the plasma near the cathode are apparent. Both arcjet designs operating at 21 kA and 6×10^{-3} kg/s had a measured terminal voltage of ~ 50 V.

B. Temperature of Argon Ions and Hydrogen Atoms, and Electron Density

The spectroscopic system was used to determine the argon ion and hydrogen particle temperature from a comparison of the observed emission profiles to Doppler-broadened profiles. If the velocities of radiating systems of mass m have a thermal distribution, then Doppler broadening results in a Gaussian line shape,

$$(1) \quad I_D(\Delta\lambda) = \frac{\epsilon(r)}{\sqrt{\pi} \Delta\lambda_D} \exp\left[-\left(\frac{\Delta\lambda}{\Delta\lambda_D}\right)^2\right]$$

where $\Delta\lambda_D = \langle v_{th} \rangle \lambda_0 / c$, where $\langle v_{th} \rangle = [2kT/m]^{1/2}$ is the most probable velocity of the emitters and $\epsilon(r)$ is the local volume emission coefficient versus radius. The emission profile for hydrogen is also affected by Stark broadening due to the presence of free electrons. The observed emission profile for hydrogen will be (in the presence of Stark and Doppler broadening) a convolution of the two line shapes and will be the well-known Voigt profile. Analysis of the Lorentzian component can be used to determine the electron density. Therefore, for measurement of the kinetic argon ion and hydrogen temperature and the electron density requires accurate determination of the respective emission profiles versus radius.

The intensity observed by the SIT-OMA from the arcjet is the integral across a cord of observation. To obtain the emission profile $\epsilon(r)$ of the arcjet plasma, it was necessary to unfold the observed intensity with a data unfolding technique. For an axisymmetric discharge, it is reasonable to assume that a volume element at a radius r is equivalent when observed at any chordal position and is therefore the same when viewed from any angle assuming that the discharge is optically thin, then the observed intensity across a cord for an axisymmetric geometry is given by:

$$I(y) = 2 \int_0^{r_0} \frac{\epsilon(r)}{\sqrt{r^2 - y^2}} r dr \quad (2)$$

where y is the vertical distance from the axis to the cord of observation. With these assumptions, a conventional Abel inversion data-unfolding technique can calculate the emission coefficient versus radius r at each observed wavelength λ . The Abel inversion technique employed in the present analysis developed by Keefer et. al., utilizes a Fourier transform technique and is effective with noisy data.^{16,17}

Time integrated line profile measurements were made through the slit in the outer conductor of the arcjet with only mid-radius gas injection of the ArII 434.803 nm line and the 696.28 nm line of hydrogen (H_α). With the system resolution, 94 radial data points are taken per discharge. The ArII emission was recorded with the spectrograph in second order and the system resolution was 0.002216 nm with a measured instrument profile that was a Gaussian with a full width at half maximum (FWHM) of 0.01262 ± 0.00045 nm. The observed signal, which is the integral across the cord of observation, was spatially filtered and also filtered versus wavelength with a low frequency bandpass with cutoff frequencies as determined by the allowable spectral frequencies from the instrument profile. The signal was then Abel-inverted at each observed wavelength to yield the arcjet emission coefficient versus radius. This produced line emission profiles versus radius that was least squares fitted to a Gaussian profile at each observed radial position in order to determine the argon ion temperature. Figure 5 shows the relative wavelength integrated intensity versus radial position from the Abel inversion. Figure 6 shows a Gaussian fit to the line emission profile at 13.6mm from the cathode with a corrected FWHM of 0.0189 ± 0.00066 nm. In general, excellent fits to Gaussian profiles were obtained at all radial positions.

Line profile measurements were also made of the hydrogen H_α emission at 696.28 nm. The observed intensity was filtered and Abel-inverted in the same manner as described for the argon data to yield line emission profiles versus radius. As previously stated, the observed line emission profiles were a convolution of Gaussian and Lorentzian profiles (Voigt profile). A de-convolution technique using inverse Fourier transforms was used to separate the line emission profile into the two components.^{18,19} No Lorentzian

component could be deconvolved for radial positions between the cathode to within 10mm of the anode. From the fit to the Lorentzian component, the electron density was calculated using standard techniques for analysis of Stark broadened H_{α} emission.^{20,21,22} The results, shown in Figure 7, indicates electron densities of $1.5 - 4 \times 10^{15} / \text{cm}^3$ for regions near the anode. Over the region between the cathode and 13mm radially, the electron density is less than approximately $1 \times 10^{15} / \text{cm}^3$.

A fit to the Gaussian component of the deconvoluted hydrogen emission profile using equation 1, indicates a particle temperature of ~ 0.5 eV, whereas, a fit to the ArII emission at the same radial and axial position indicates a argon ion temperature of 13.6 eV. The two measurements are in sharp disagreement indicative of the presence of gross mass motion and microturbulence in the plasma.²¹⁻²² In order to estimate the extent to which one would expect the hydrogen and argon ions to achieve the same temperature and flow velocity in the experiments, the time for energy equipartition assuming classical coulomb collisions only was calculated. From Spitzer, the equipartition time is,²³

$$t_{eq} = \frac{5.87 A A_f}{n_f Z^2 Z_f^2 \ln \Lambda} \left(\frac{T}{A} + \frac{T_f}{A_f} \right)^{3/2} \quad (3)$$

where, n_f = density of *field* particle in cm^{-3} ,

A, A_f = atomic masses of *test* and *field* particles [AMU],

Z, Z_f = ionic charge,

$\ln \Lambda$ = coulomb logarithm, and

T, T_f = temperatures in $^{\circ}\text{K}$. For particle densities inside the thrust chamber of $\sim 10^{15} / \text{cm}^3$, and electron temperature on the order of ~ 1 eV, then the equipartition time is 30 ns. At flow speeds of $\sim 10^4$ m/s, the characteristic discharge length for equipartition is then $\delta \approx 0.3 \text{ mm}$, which is less than the measurement window ($\geq 1 \text{ mm}$). Therefore, the hydrogen and argon are expected to be better coupled in velocity space than indicated from particle temperatures calculated from the measured Gaussian emission profiles.

C. New Technique for Measurement of Speed, Turbulence, and Temperature

As discussed previously, the integrated light intensity accumulated along a succession of chordal views of an axisymmetric object is usually converted to an emission intensity per unit volume distribution with respect to the cylindrical radius by means of

the Abel inversion. This technique is quite reasonable in converting the total intensity (over all wavelengths) from a function of position (perpendicular to both the symmetry axis and the chordal view) into a function of cylindrical radius. At any particular wavelength, however, the contributions by emitters moving toward or away from the observer along the chordal view depends on the angle of the view relative to the cylindrical radius. That is, the Doppler shift of radiation at some point in the line profile appears for those portions of the cylindrical distribution whose radial speed aligns with the chordal view. For a chord that just grazes a particular cylindrical shell (in an azimuthally symmetric distribution of intensity and velocity) the Doppler shift is negligible. The width of a spectral line, however, will still have contributions due to random particle motions due both to the plasma temperature (heavy-particle) and hydrodynamic turbulence. Figure 8 schematically illustrates the observation geometry for an axisymmetric flow and the contributions to the observed intensity profile from an emission element at \mathbf{r}' from two different chordal positions, \mathbf{y} and \mathbf{y}' . If there are velocity components from the volume element $d\mathbf{V}$ along the line of sight that are due to radial plasma motion, then the observed intensity at \mathbf{y} and λ from $d\mathbf{V}$ will be shifted to $\pm \lambda_0(v_r \sin \theta)/c$ at \mathbf{y}' . The volume element emission coefficient will then be given by:

$$\epsilon(r, \lambda) = \frac{\epsilon(r)}{\sqrt{\pi} \Delta\lambda_D} \exp \left[- \left(\frac{\Delta\lambda \pm \lambda_0 \frac{v_r \sin \theta}{c}}{\Delta\lambda_D} \right)^2 \right] \quad (4)$$

where θ is the angle from vertical to the velocity vector at \mathbf{r} and \mathbf{y} , and $\epsilon(r)$ is the integral of the local emission coefficient over all wavelengths. Therefore for an emitting gas with radial velocity components, a standard Abel unfolding technique to solve for $\epsilon(r, \lambda)$ would yield inaccurate emission profiles.

It is not possible to separate the effects of radial speed in the plane perpendicular to the symmetric axis for arbitrary (albeit, axisymmetric) radial distributions of plasma density, speed and temperature using direct Abel inversion of chordal data. Instead, however, a new procedure can be followed in which Abel inversion of chordal path for the total intensity of a line (integrated over all wavelengths) is first used to obtain the total emission intensity as a function of radius, $\epsilon(r)$. This distribution of total intensity then

provides the amplitude factors for a succession of nested cylindrical annuli intercepted by a chordal view. Each annulus contributes to the radiation received by the chordal view at any wavelength in a manner that depends on the emission profile in the annulus, and the components of radial speed along the chord as determined by geometry. The outermost annulus, however, is only grazed by a chordal view, so its contribution at any wavelength is related only to the random plasma speed. Thus, the outermost annulus emission profile will be observed to be centered around the true line center, λ_0 . For the adjacent chordal view (closer to the symmetry axis), contributions are received from the next inner annulus, that is also observed with the apparent line center around λ_0 with a emission profile a function of random plasma speed at that radius just grazed by the chord, and the outer annulus which has both a spread (due to the previously established random speed) and a shift (on either side of the line center) associated with the component of radial speed along the chord by plasma in this annulus. Two unknowns are, therefore, present at each chord: the spread due to random motion for the annulus just grazed; and the shift due to the component of radial speed in the next outboard annulus. Note that with the absolute (total) emission intensity at each radius, $\epsilon(r)$ is known using an Abel inversion technique as previously described from wavelength integrated chordal intensity data. A two-parameter, least-squares curve fit is performed in which two curves are added: a Gaussian with the known emission $\epsilon(r)$ and an unknown $\Delta\lambda_D$ (but $v_r \sin\theta = 0$) and a curve consisting of two equal Gaussians with emission $\epsilon(r')$, widths $\Delta\lambda_D(r')$, but unknown shifts (+/-) about $\lambda = \lambda_0$, due to the unknown value of $v_r(r')$.

Application of this unfolding technique to the argon ion and hydrogen data for mid-radius gas injection only was used to calculate the true emission profile versus radius in the presence of radial velocity components and to yield a solution for v_r versus radius. Figure 9 shows the radial velocity component versus radius for this arcjet geometry with mid-radius gas injection. The results indicate radial flow on the order of 10^4 m/s with a peak speed of 1.25×10^4 m/s.

For a fully developed turbulence, the velocity distribution can be approximately described by a Gaussian distribution.^{24,25} If the thermal and turbulent velocity motions are uncorrelated then the unfolded emission profile in the presence of turbulence will represent the convolution of two Gaussian distributions, (one thermal and one turbulent) and the parameter $\Delta\lambda_D$ is related to the thermal and turbulent components by,²²

$$\Delta\lambda_D^2 = \left(\frac{\lambda_o}{c} \langle v \rangle_r \right)^2 + \left(\frac{\lambda_o}{c} \sqrt{\frac{2kT}{m}} \right)^2 \quad (5)$$

where $\langle v \rangle_r$ is the mean turbulent velocity and T is the gas kinetic temperature. If two constituents in the flow of different mass have a common temperature and a common turbulent velocity component, then equation 5 gives a system of two equations that can be solved for T and $\langle v \rangle_r$ from the unfolded values of $\Delta\lambda_D$ versus radius.

Results of the analysis of the previously calculated emission profiles versus radius for argon and hydrogen using equation 5 are shown in upper curve in Figure 10. This calculation has indicated particle temperatures of ~ 0.5 eV in the midplane to anode region with an $\sim 50\%$ rise in temperature toward the cathode. The hydrodynamic turbulent velocity, (shown in the lower curve in Figure 10) shows a rise of nearly 300% from $1.5 \cdot 10^3$ m/s in the midplane to anode region to about $7 \cdot 10^3$ m/s near the cathode.

As discussed previously, two MPD arcjet configurations were studied. A second design for gas injection with 50% at mid-radius and 50% at the cathode base was prompted by the apparent deposition in the original design of copper and tungsten on the boron nitride insulator in regions near the cathode. The observed chordal emission profiles with the new gas injection design were significantly less broadened than the previous design. Therefore, time integrated measurements through the slit in the outer conductor of the 434.8 nm argon ion line were made with the spectrograph in third order providing an increase in wavelength resolution of 0.00113 nm/pixel. The measured instrument profile had a FWHM of 0.0043 ± 0.00012 nm. The new Abel inversion technique was then used to analyze the observed 434.8 nm argon ion and hydrogen H_α intensity. These results are shown in Figures 11 and 12. The plasma in the thrust chamber with the new gas injection design has radial velocity components on the order of $3 \cdot 10^3$ m/s with near zero velocity observed 12.5 to 17.5 mm from the cathode. These measured radial speeds are approximately a factor of three less than observed in the original arcjet design. Application of equation 5 to the corrected emission profiles for argon ion and hydrogen emission indicates little or no detectable hydrodynamic turbulence and particle temperatures on the order of 0.3 eV. However, the new design for gas

injection causes the particle temperature to rapidly increase near the outer conductor to ~0.9 eV.

V. MHD CODE RESULTS

In addition to the experimental effort, a short series of numerical code simulations of the MPD thrust chamber flow have been performed to provide some initial indication of flow field behavior, and also to evaluate the ability of the existing MACH2 computer code¹⁵ to handle MPD arcjet problems. The MHD code MACH2 is a one-temperature, single fluid code with three magnetic field components. It includes an Arbitrary-Lagrangian-Eulerian (ALE) mesh with adaptive grid control, perfect gas or tabular equations of state, thermal and magnetic field diffusion, radiative emission, and the Hall effect. The initial calculations were made with coarse zoning and gave reasonable agreement with the experimental magnetic field measurements.

Figure 13-16 display results from the MACH2 code for conditions resembling those of the experimental tests, in terms of electrode dimensions, total current, and total mass flow rate. For simplicity in the limited effort available, the mass flow is injected uniformly through the insulator backplate, and the cathode is truncated sharply at the anode exit plane. The current contours shown in Fig. 13 resemble those for the first arcjet (mid-radius only injection) in regard to the retention of current flow within the thrust chamber. With uniform mass injection, there is no indication in the code results of an inflection of the current streamlines at mid-radius.

At an axial position corresponding to the measurement station of the spectroscopic studies, the single-temperature code computes a temperature that rise from about 1.4 to 2.8 eV in traversing from the anode to the cathode. While these values are significantly higher than estimates from spectroscopic study of the first arcjet configuration, the increase in temperature toward the cathode is similar. A decrease in particle density, density values in the range of 10^{15} cm^{-3} , radially inward from the anode is also implied by both the code and the earlier Stark broadening data. The velocity vectors shown in Figure 16 have maximum computed values $3.5 \times 10^4 \text{ m/s}$, for very low density flow in the thruster exhaust. Within the thrust chamber itself, maximum total speeds are about $2.4 \times 10^4 \text{ m/s}$, in the low density flow approximately one-third of the inter-electrode gap

from the cathode surface.

The calculated flow field within the thrust chamber has the appearance of plasma expanding from a relatively high pressure region near the cathode base, while constrained to curve axially downstream under the influence of the electromagnetic forces in the discharge. At the measurement station, this flow field would exhibit a maximum radial speed at about 6.4 mm from the cathode surface, in good agreement with experimentally-derived distribution. (The code calculation, however, indicate a radial speed at this position of about 5 km/s, which is less than half of the spectroscopic results.) Close comparison of computational and experimental results would require more extensive modeling, and measurements at additional axial stations, in order to discern differences that are due only to variances in exact geometry or location. A moderate amount of further code development would also be useful to allow for nonequilibrium conditions, (e.g., electron versus heavy-particle temperatures), and electrode boundary effects.

VI. CONCLUSIONS

In order to understand and improve the performance characteristics of MPD arcjets, it is necessary to determine the electromagnetic discharge and flow structures within the thrust chamber and their relationship to the arcjet design and operating conditions. The present research program has analyzed in detail two MPD thrust chambers by measurement of the electromagnetic field distributions, particle densities and velocities in the thrust chamber flow. A new technique was developed to unfold the emission distribution and profile and to estimate thermal, radial and (in-plane) turbulent velocity components. The results indicate that the plasma within the MPD arcjet with only mid-radius gas injection has a strong radially-inward flow with a substantial increase in hydrodynamic turbulence near the cathode. Analysis of a second MPD arcjet with 50% mid-radius gas injection and 50% at the cathode center conductor indicates significantly reduced radial velocities. In addition, the observed hydrodynamic turbulent velocities are reduced by a factor of five along with significantly reduced kinetic temperatures in the chamber.

The measured radial mass flow and development of hydrodynamic turbulence would have important consequences for thrust efficiency since shock and viscous losses near the cathode surface would be expected. It may also be expected that the relative strength of the radial (versus axial) flow can change significantly as the total current and mass flow values are varied with fixed electrode configuration and injection geometry. Such change in flow direction can substantially affect the MPD thruster performance for reasons that cannot be inferred from simple scaling relationships based on electromagnetic thrust and total mass flow. Examination of MPD performance by variation of operating current and mass flow rate, (i.e., external parameters) with a fixed device geometry will thus be an inaccurate procedure for assessing the potential of MPD thrusters. Instead, it will be necessary to vary the arcjet geometry and/or mass-inlet ratios as the current is changed. To guide the combination of geometry, current and mass flow toward an optimum design, two-dimensional calculations are required.

VII. REFERENCES:

1. Ducati, A. C., Gianninin, G. M., and Muhlberger, E., "Experimental Results in High-Specific-Impulse Thermo-Ionic Acceleration," *AIAA Journal*, Vol. 2, No. 8, Aug. 1964, pp. 1452-1454.
2. Patrick, R. M. and Schneiderman, A. M., *AIAA Journal*, Vol. 4, 1966, p. 283.
3. Fradkin, D. B., et. al., *AIAA Journal*, Vol. 8, 1970.
4. Clark, K. E. and Jahn, R. G., *AIAA Journal*, Vol. 8, 1970.
5. Michels C. J. and Sigman, D. R., *AIAA Journal*, Vol. 9, 1971.
6. Malliaris, A. C., et. al., *AIAA Journal*, Vol. 10, 1972, p. 121.
7. Jahn, R. G., *Physics of Electric Propulsion*, McGraw-Hill, New York, 1968, Chapter 8.
8. Turchi, P. J., and Jahn, R. G., *AIAA Journal*, Vol. 9, 1971, p. 1372.
9. Jahn, R. G., Clark, K. E., Oberth, R. C. and Turchi, P. J., "Acceleration Patterns in Quasi-Steady MPD Arcs," *AIAA Journal*, Vol. 9, No. 1, Jan 1971, pp. 167-172.
10. Kribel, R., Eckdahl C., and Lovberg, R., *AIAA Journal*, Vol. 9, 1971.
11. Oberth, R. C. and Jahn, R. G., *AIAA Journal*, Vol. 10, 1972.
12. Bruckner A. P. and Jahm, R. G., *AIAA Journal*, Vol. 12, 1974, p. 1198.
13. Aeschliman, D. P. and Evans, D. L., *J. Quant. Spectroscopy and Rad. Transfer*, Vol. 16, 1976, p. 191.
14. Heimerdinger, D. J., et. al., "Effects of Axial Variation of Electrode Spacing on MPD Arcjet Behavior", 19th International Electric Propulsion Conference, Colorado Springs, CO, May 11-13, 1987.
15. Buff, J., et. al., *IEEE Transactions on Plasma Science*, Vol. PS-15, 1987, p. 766.
16. Keefer, D. R., et. al., *J. Quant. Spectroscopy and Rad. Transfer*, Vol. 39, 1988, p. 367.
17. Smith, L. M., *IEEE Transacitons on Information Theory*, Vol. 34, 1988, p. 158.

18. Harris, K. L., J. Optical Soc. of America, Vol. 56, 1966, p. 569.
19. Helstrom, C. W., J. Optical Soc. of America, Vol. 57, 1967, p. 569.
20. Wiese, W. L., in Plasma Diagnostic Techniques, eds. R.H. Huddleston and S. L. Leonard, Academic Press, NY, 1965, Chapter 6.
21. Traving, G., in Plasma Diagnostics, ed. W. Lochte-Holtgreven, North Holland Publishing, Amsterdam, 1968, Chapter 2.
22. Griem, H. R., Plasma Spectroscopy, McGraw-Hill, NY, 1964, Chapter 4.
23. Spitzer, L. Physics of Fully Ionized Gases, Interscience, NY, 1962, Chapter 5.
24. Zhi, G. and Qian, J., Applied Optics, Vol. 26, 1987, p. 1956.
25. Hinze, J. O., Turbulence, McGraw-Hill, NY, 1975.
26. Turchi, P.J., et. al., IEEE Transactions on Plasma Science, Vol. PS-15, 1987, p. 747.

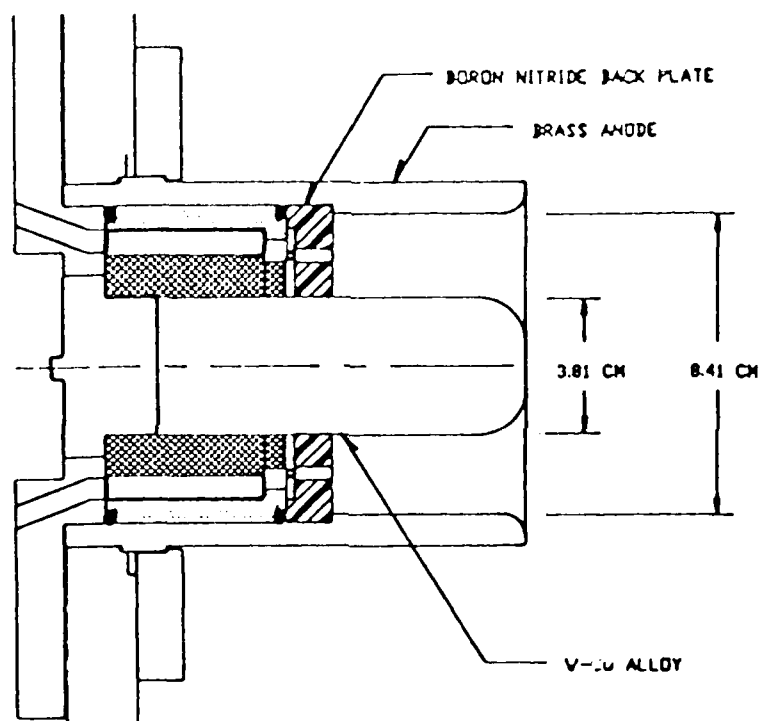


Figure 1. Schematic of MPD arcjet for study of MPD thrust chamber flow dynamics. Gas injection is through 16 choked orifices at mid-radius in boron nitride backplate.

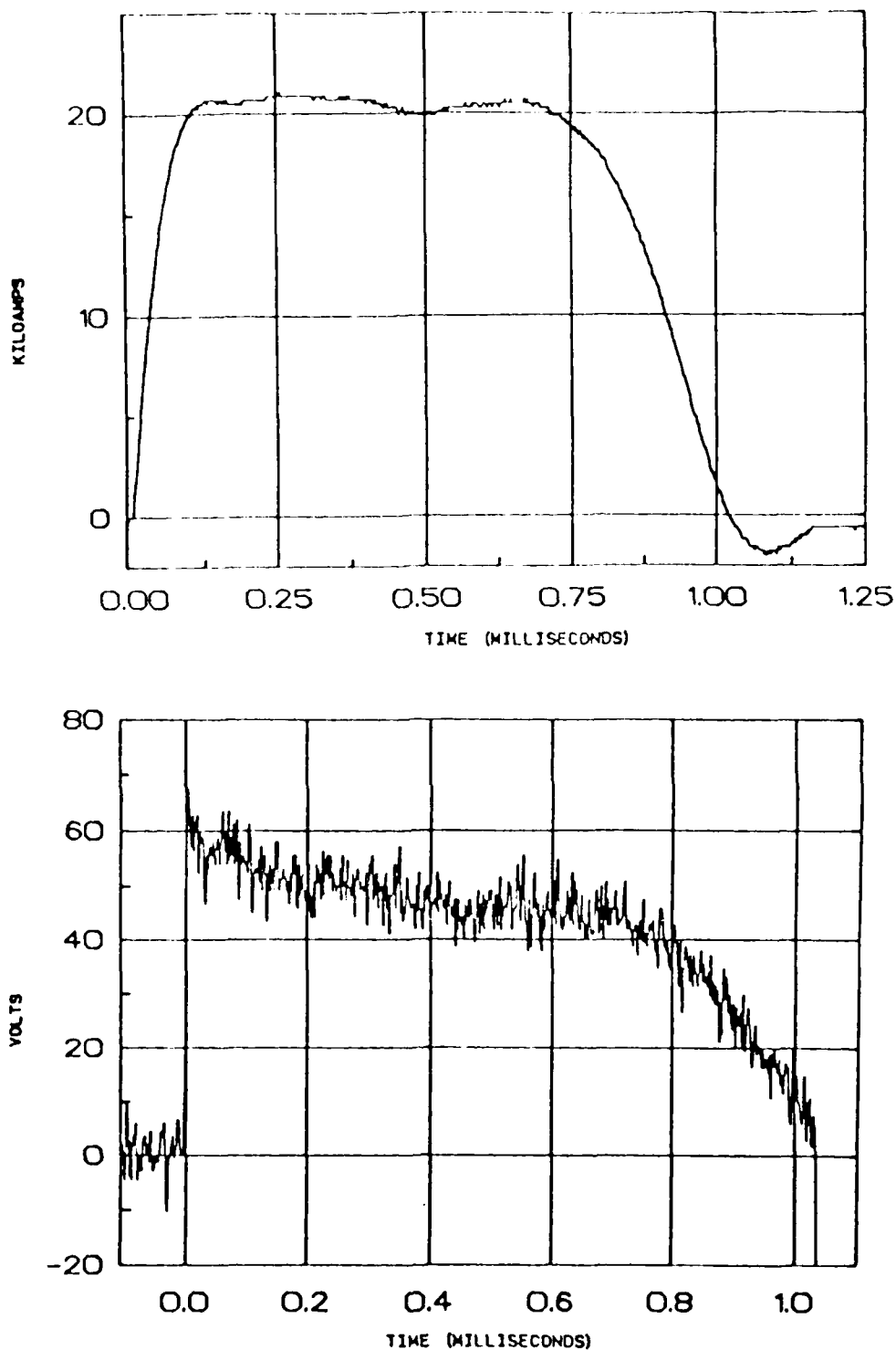


Figure 2. MPD arcjet operating characteristics: a) current delivered to the MPD arcjet has a FWHM of 0.88 ms with a risetime of 0.1 ms. An initial charge of 8 kV on the LC-ladder capacitor bank gives a current of approximately 21 kA; b) terminal voltage at the arcjet (not corrected for inductive voltage transients) attains a quasi-equilibrium value about 0.2 ms after current initiation.

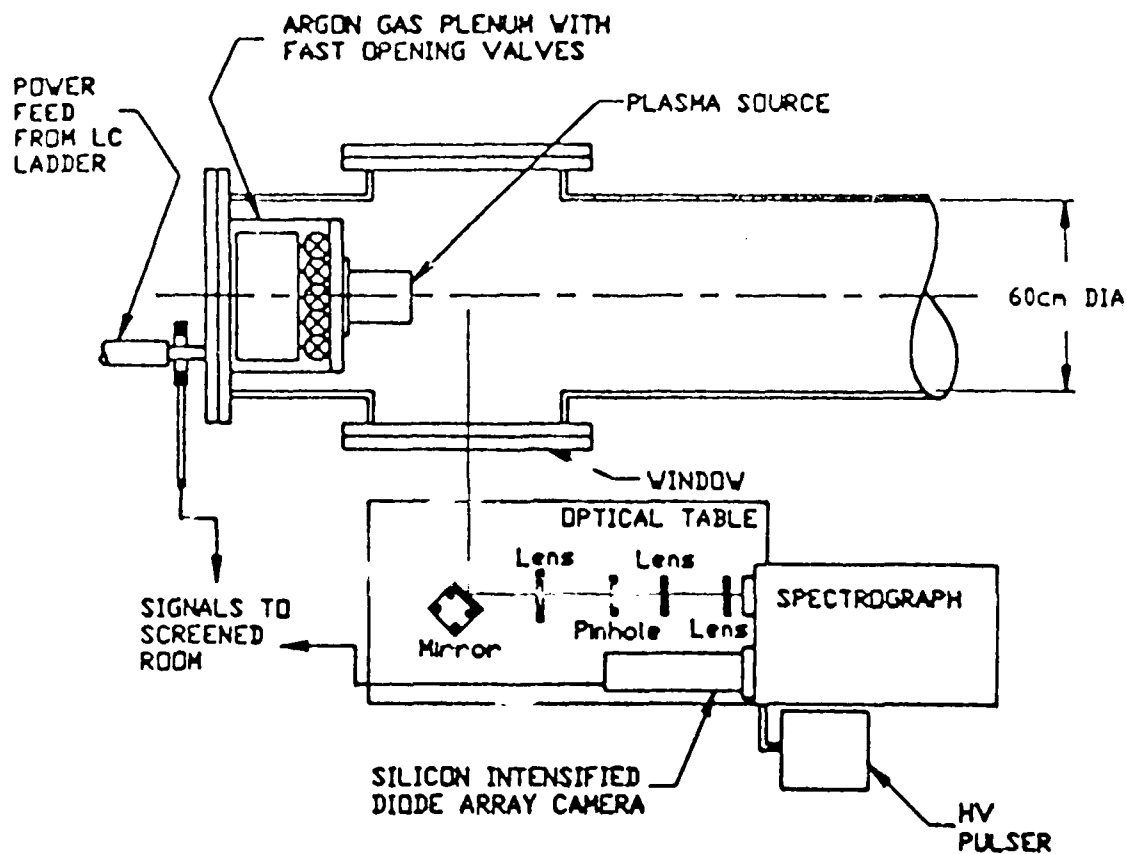


Figure 3. Basic layout of the MPD arcjet experiment. In the present experiments, the line of sight is actually through slits in the outer electrode of the thruster.

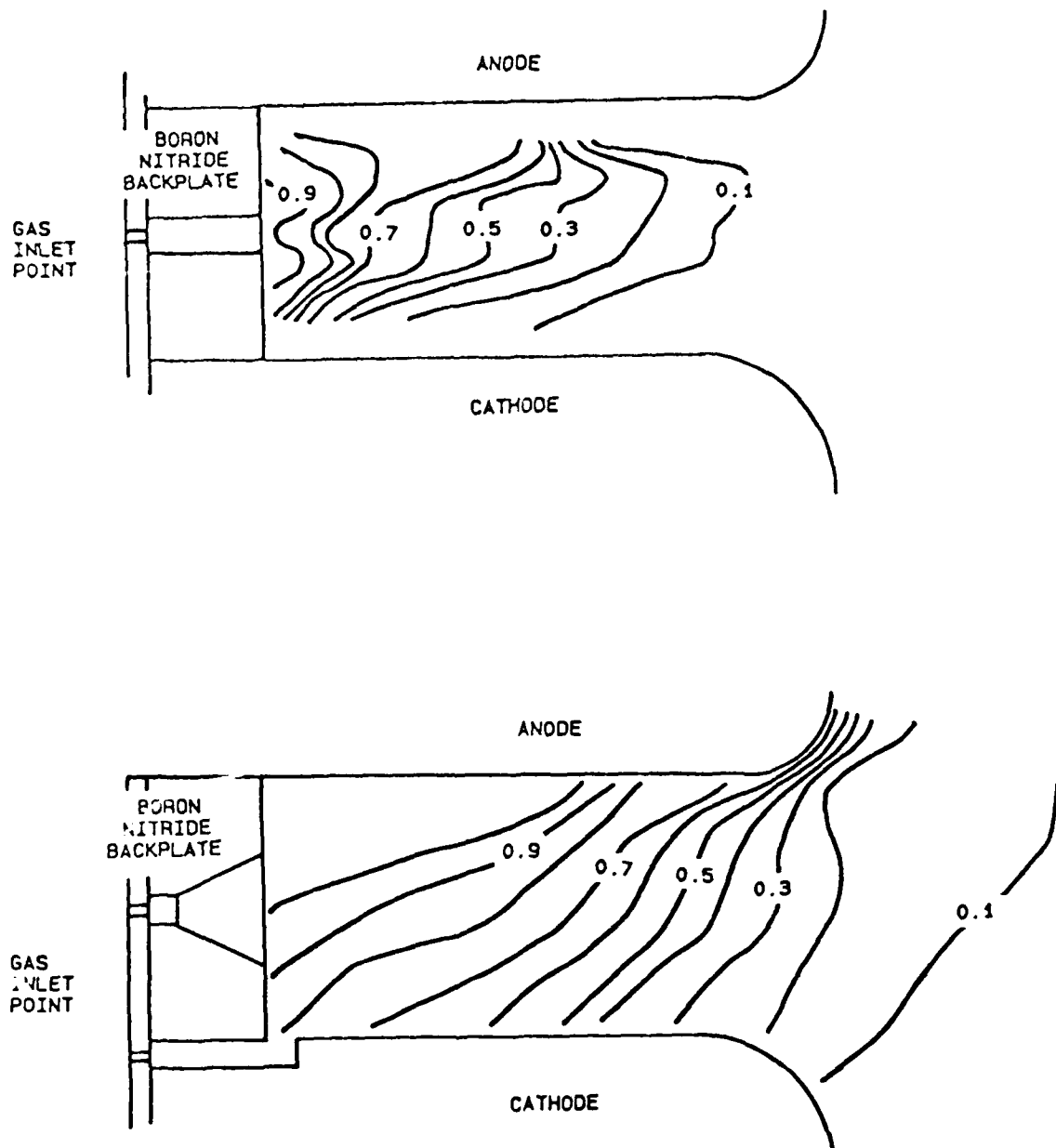


Figure 4. Current contours in the MPD arcjet operating at 21 kiloamps and 6×10^{-3} kg/s; a) for the case of mass injection only at mid-radius indicates that the current does not fill the thrust chamber and has radial force components towards the cathode center conductor, b) for the case of 50% mass injection near the cathode base and 50% at mid-radius indicates more than 20% of the current external to the thrust chamber with reduced radial force components.

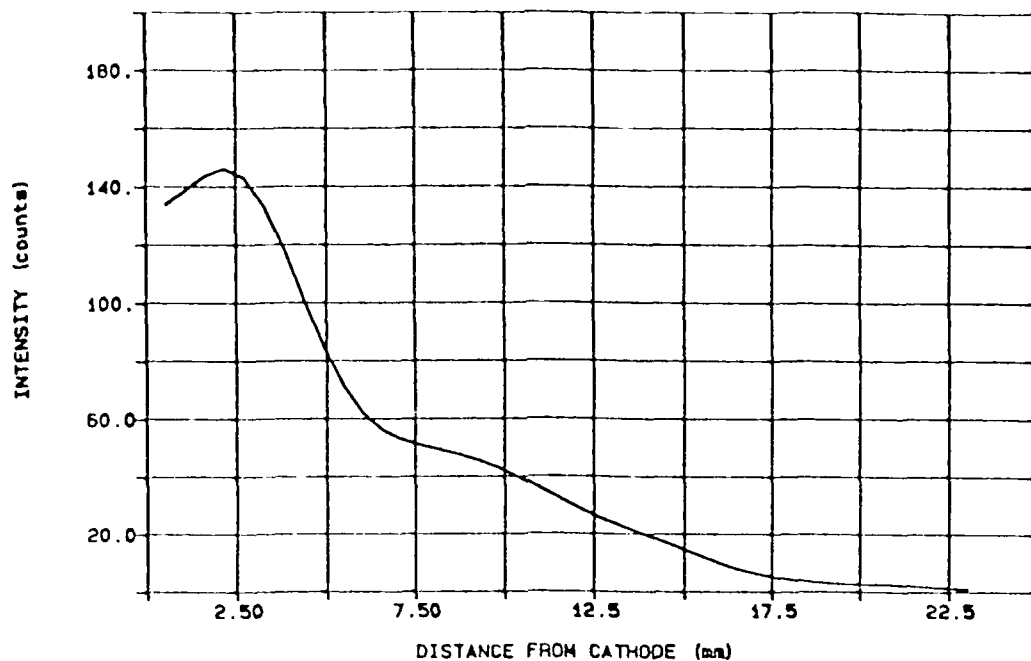


Figure 5. Relative intensity of argon ion emission (integrated over the line profile) versus radial position from Abel inversion of Ar II 434.803 nm emission is peaked toward the cathode at 19.05 mm) and monotonically decreases.

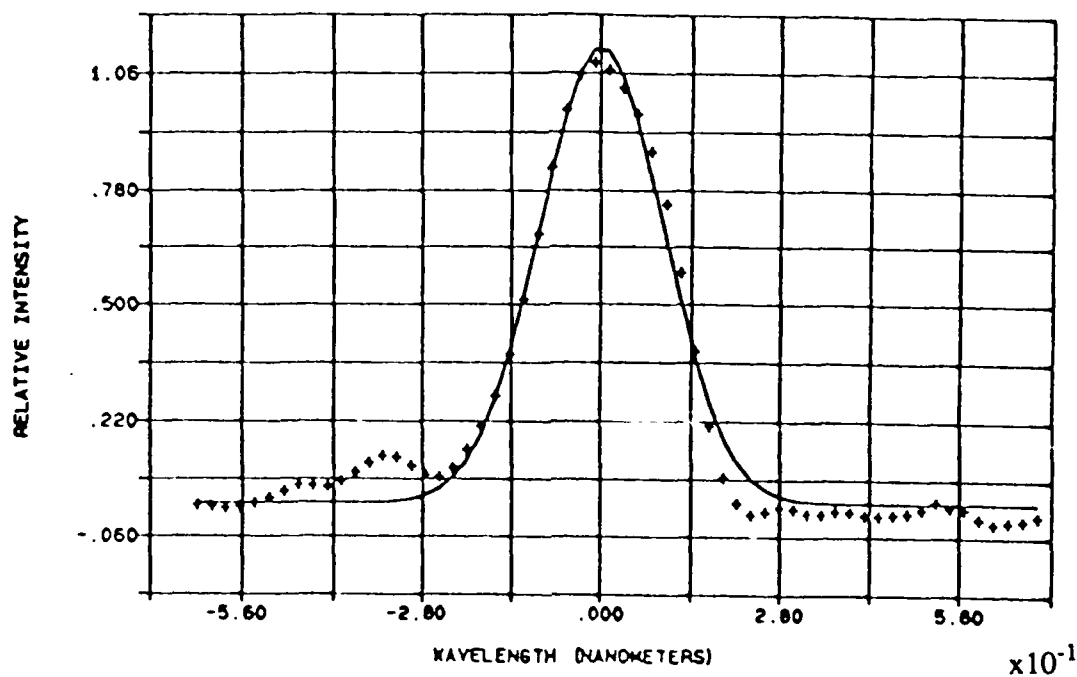


Figure 6. Line profile of Ar II line at 13.6 mm from the cathode surface. Least-squares fit to a Gaussian profile is also shown.

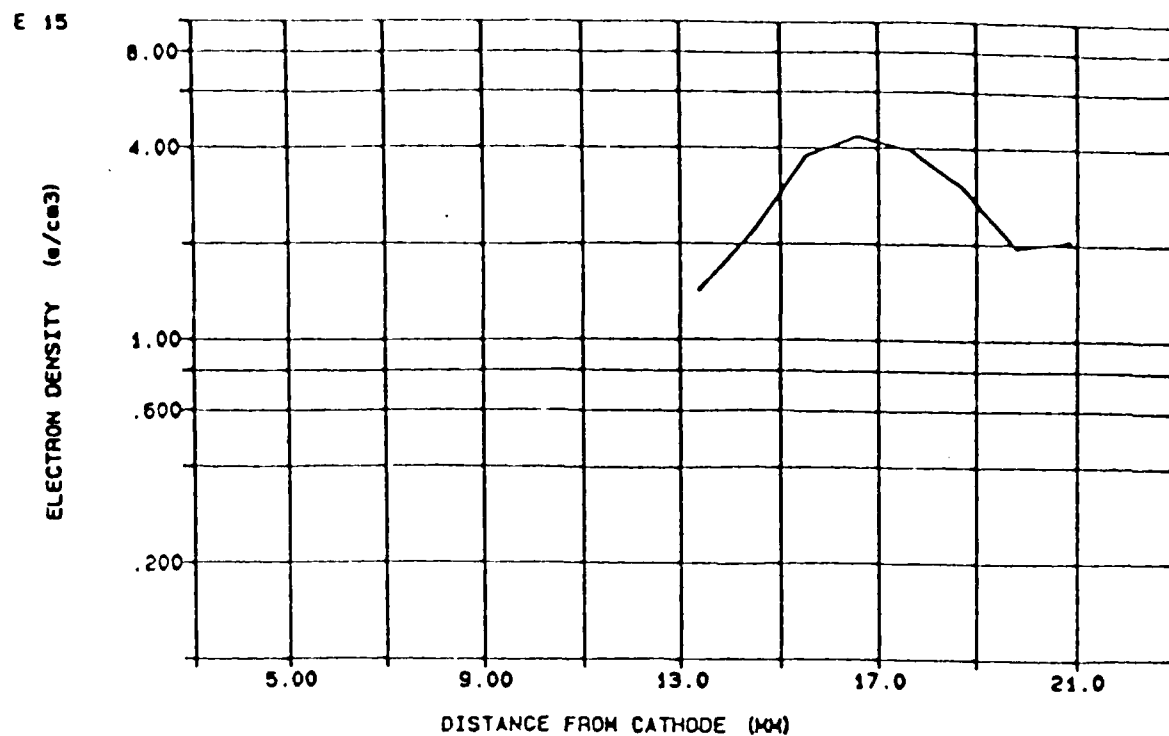


Figure 7. Calculated electron density versus distance from the cathode from Lorentzian component of line profile fit to hydrogen 696.28 nm emission.

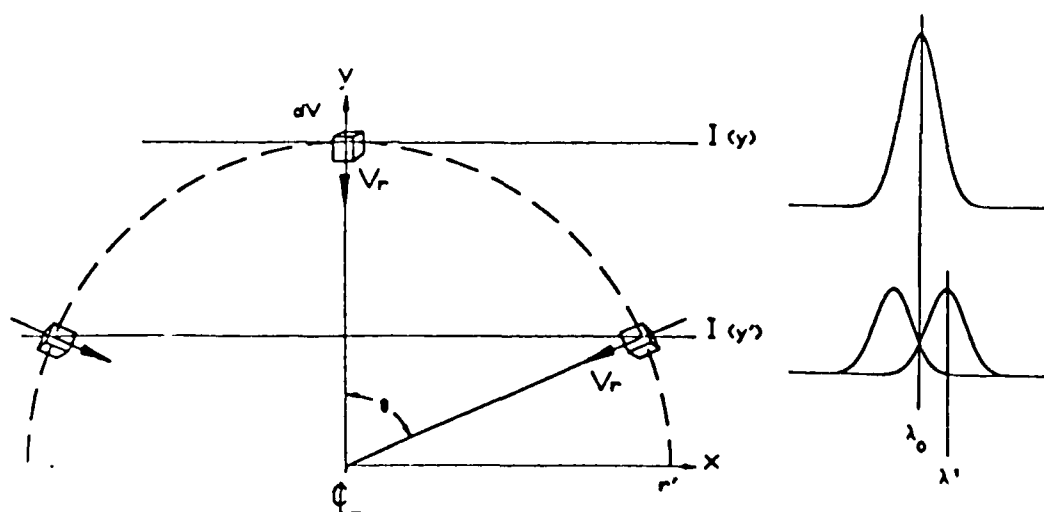


Figure 8. The emission profile versus wavelength from an axisymmetric flow from equivalent differential volume elements a y and y' will not be equal in the presence of radial velocity components. The emission profile at y' will be Doppler shifted to $\pm \lambda_0 V_r \sin \theta / c$ where λ_0 is the line center.

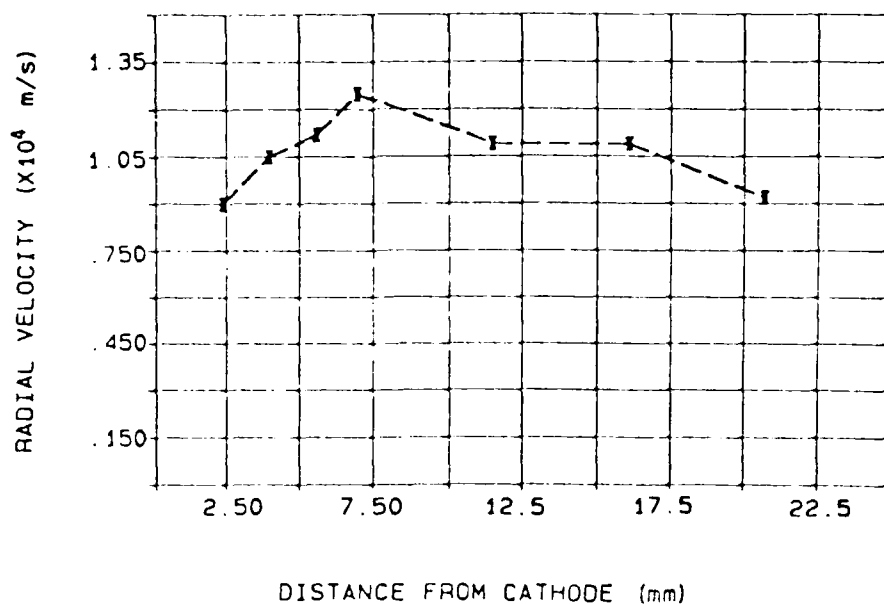


Figure 9. Application of new diagnostic technique in the study of the internal flow dynamics of an MPD arcjet with a cathode center conductor and inner electrode spacing of 2.3 cm for the case of mid-radius only mass injection shows radial velocities on the order of 10 km/s.

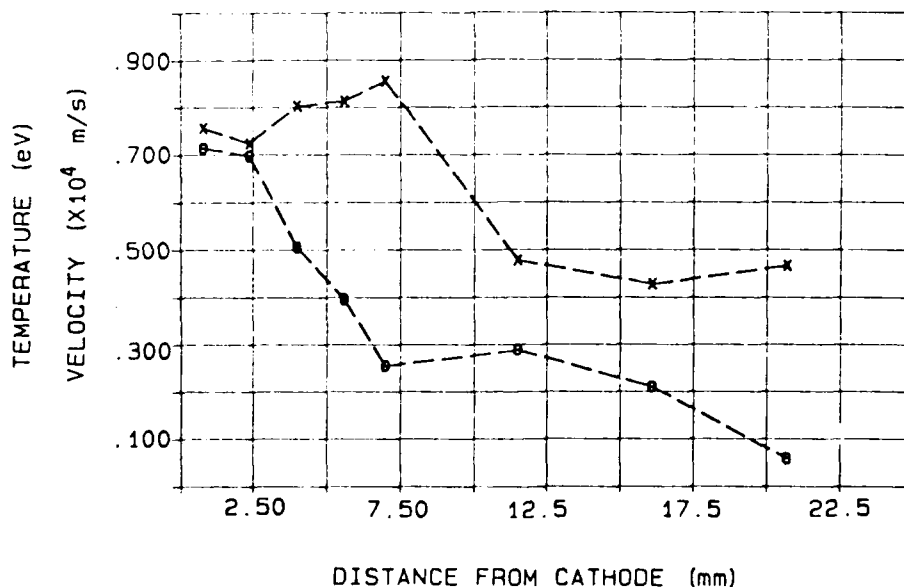
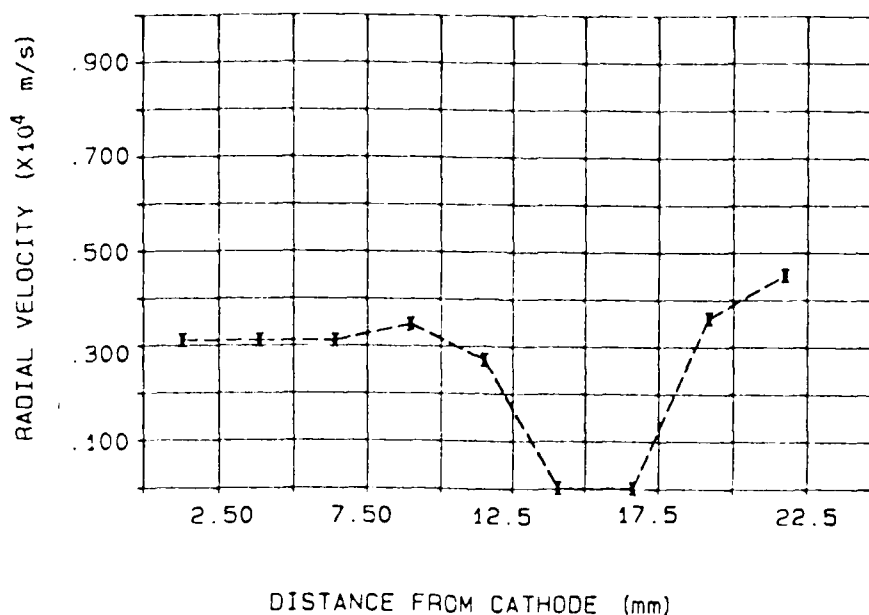
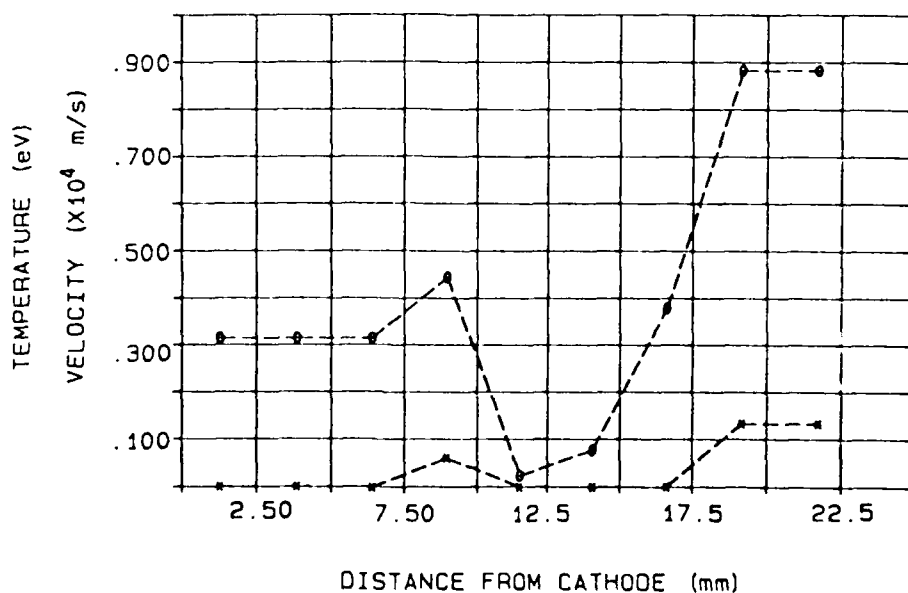


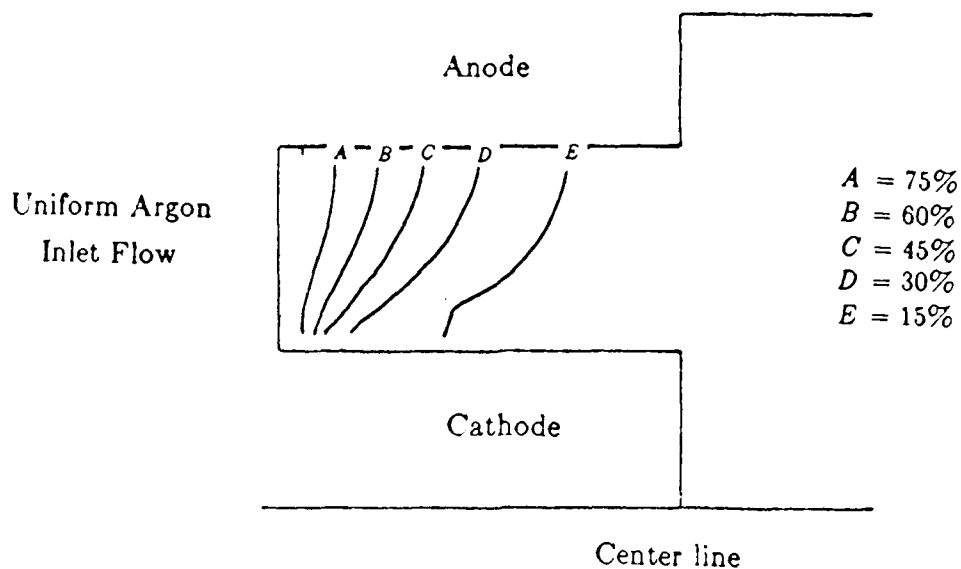
Figure 10. Distribution of gas temperature (upper curve) and turbulent speed (lower curve) for the case of mid-radius only mass injection, based on both argon and hydrogen emission analysis.



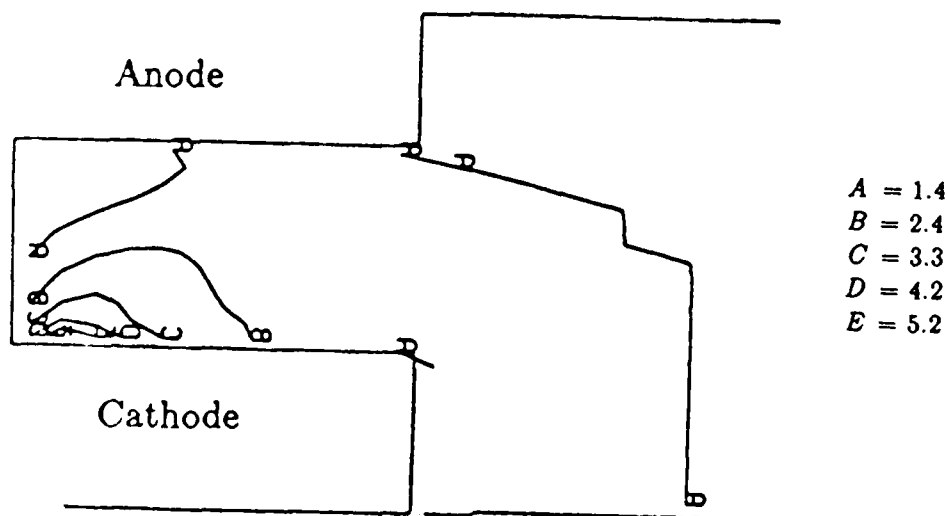
11. Application of new diagnostic technique in the study of the internal flow dynamics of an MPD arcjet with a cathode center conductor and inner electrode spacing of 2.3 cm for the case of 50% mass injection at cathode base and 50% at mid-radius shows radial velocities on the order of 3 km/s.



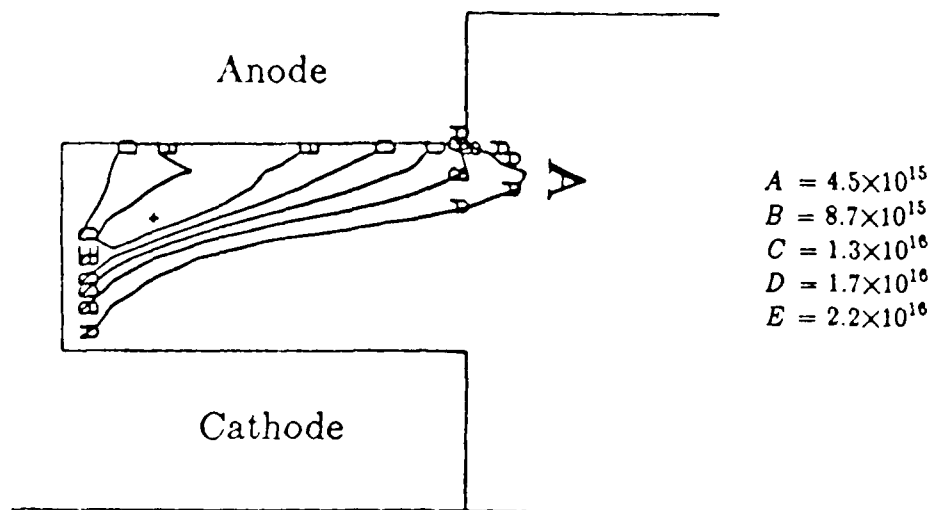
12. Distribution of gas temperature (upper curve) and turbulent speed (lower curve) for the case of 50% mass injection at cathode base, based on both argon and hydrogen emission analysis indicates reduced turbulent speeds to less than 1 km/s.



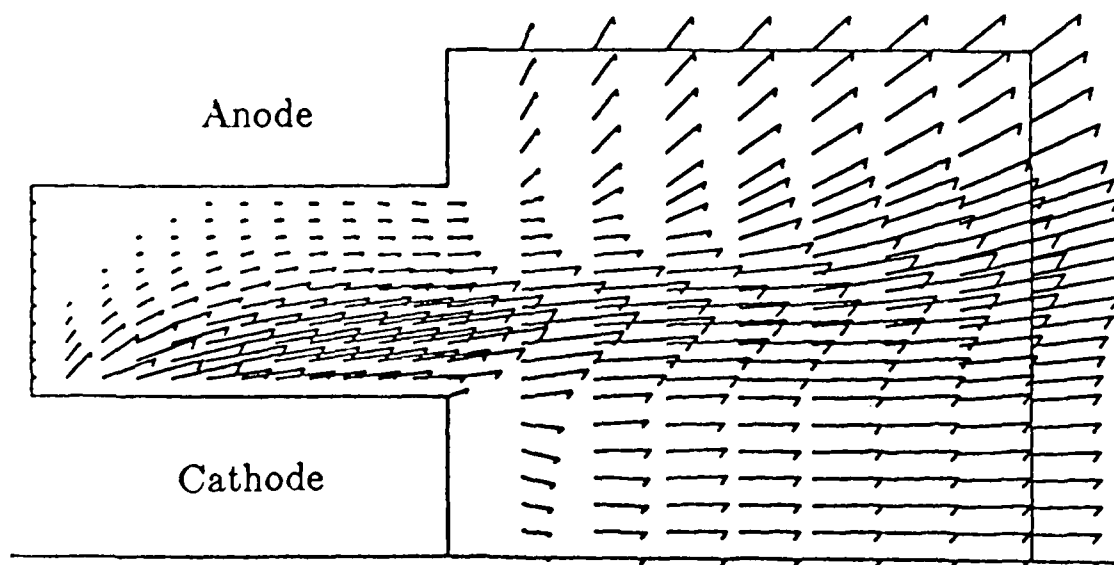
13. Current contours calculated by MACH2 computer code for case of uniform mass injection (at 6 g/s) through insulator backplate. Total current in 21 kA.



14. Constant temperature contours in units of (eV) calculated by MACH2 computer code for case of Fig. 13.



15. Constant atom number density contours in units of cm^{-3} calculated by MACH2 computer code for case of Fig. 13.



16. Distribution of flow velocity calculated by MACH2 computer code for case of Fig. 13. Magnitude of longest vector (well downstream of cathode corner) is 3.5×10^4 m/s.

VIII. APPENDIX



AIAA-90-2664
MPD Arcjet Thrust Chamber
Flow Studies

P.J. Turchi, Ohio State Univ.
Columbus, OH

J.F. Davis, R&D Associates, Inc.
Alexandria, VA

N. Roderick, Univ. of New Mexico
Albuquerque, NM

AIAA/DGLR/JSASS
21st International Electric Propulsion Conference
July 18-20, 1990 / Orlando, FL

MPD THRUST CHAMBER FLOW DYNAMICS

P.J. Turchi, Ohio State University
J.F. Davis, R & D Associates, Inc.
N.F. Roderick, University of New Mexico

ABSTRACT

Flow within the thrust chamber of an MPD arcjet is examined experimentally, and modeled with a two-dimensional MHD code. Two quasi-steady MPD thrusters are considered under the same input conditions of current (31 kA) and total mass flow rate (6×10^{-3} kg/s, argon + 1.5% hydrogen). The arcjets have the same basic design, consisting of a central cathode, 3.8 cm diam and 5 cm long, separated from a coaxial anode of equal length by a uniform gap of 2.3 cm. Two different mass injection arrangements are used (100% at mid-radius, and 50% at the cathode base, with the remainder at mid-radius). A new spectroscopic analysis procedure is developed that allows distributions of radial speed, heavy-particle temperature, and (in-plane) turbulent speed to be extracted from chordal measurements of light emission by the two species in the plasma flow. Good qualitative (and reasonable quantitative) agreement exists with distributions calculated by the MHD code, indicating that flow within the thrust chamber expands from an electromagnetically-pumped plasma layer extending downstream of the cathode base (vs a pumped jet off the cathode tip). The significant variation of internal flow dynamics with mass injector arrangement implies the need for extensive experimentally-validated code modeling in order to evaluate the potential performance of MPD thrusters.

INTRODUCTION

For the last twenty-five years, there has been continued interest in the so-called magnetoplasmadynamic (MPD) arcjet. Operation of an arcjet in the MPD mode was discovered by A. Ducati in the course of research on arcjet performance in which he lowered the input mass flow rate to the thrust chamber, and found that a relatively benign discharge condition could be achieved¹. Rather than leading to higher chamber temperatures, with increased erosion of the electrodes, the reduction in mass flow rate provided increased lifetime, higher specific impulse, and (for hydrogen, at least) higher efficiency. These improvements were accomplished in a device that retained the simplicity of conventional arcjets in regard to construction, parts-count, and power supply requirements. Subsequent studies extended operation to propellants other than hydrogen, and included various arrangements of auxil-

iary magnetic fields, and electrode geometries²⁻⁶. MPD arcjet became an appellation for devices ranging from steady conventional arcjets (operating at higher currents and/or lower mass flow rates than thermal arcjets), pulsed high current discharges (descended from plasma-pinch engines), and crossed-field Hall accelerator arrangements⁷. Along with the broadening of the MPD arcjet category (which at best might recognize a commonality of physical mechanisms or concerns) came a profusion of theoretical models and experimental data, which were often consistent within individual devices, but in conflict when applied across the entire class of thrusters. The difficulty of probing within the small (~few mm) chamber dimensions of steady-state devices, and the need to identify thruster arrangements/regimes with attractive performance values has involved a concentration on terminal measurements, such as current, voltage, and thrust. Detailed diagnosis of the structure of the discharge and flow within the thrust chamber has been attempted only in the higher power (~megawatt) quasi-steady laboratory devices⁸⁻¹⁴, and even then, only for a limited range of operating conditions.

The particular difficulties with understanding MPD arcjet performance in terms of the actual thrust and energy transfer mechanisms within the arcjet chamber have been two-fold: an inability to monitor experimentally changes in flow structure with variation in terminal conditions; and an inability to model accurately the two-dimensional, electromagnetically-powered discharge flow. The present paper discusses progress in overcoming these difficulties in terms of a new spectroscopic technique for obtaining thrust chamber flow conditions, and the application of a two-dimensional MHD code developed originally for pulsed, coaxial plasma gun modeling¹⁵.

EXPERIMENTAL APPARATUS

Experimental Technique and Equipment

At the R & D Associates Washington Research Laboratory, the experimental facility for study of MPD arcjets uses a stainless steel vacuum tank, 6.0 m long and 0.61 m inside diam, as a vacuum plenum for quasi-steady arcjet operation. Attached to the upstream end of this tank are diagnostic sections with 35.6 cm diam ports for optically-clear views through the test section, including chordal access through the arcjet anode. Use of a separate diffusion pump (2000 l/s) at each end of the vacuum plenum establishes an initial background pressure of about 1.5×10^{-6} torr. The basic layout is shown schematically in Fig 1.

Two MPD arcjets, differing only in mass injector configuration, have been used for the study of internal flow

dynamics: 1) all mass flow through orifices at mid-radius, as shown in Fig 2b; and 2) half the mass flow through orifices at mid-radius (with more open transition to the thrust chamber), and the remainder of the mass flow through orifices opening to a circular groove surrounding the cathode base. The latter arrangement (shown in Fig 3b) was prompted by the apparent deposition of cathode material on the boron-nitride insulator after extensive use of mid-radius-only injection. Both arcjet configurations have a brass outer anode, and a copper-tungsten alloy cathode. The inter-electrode gap is 23 mm, and the channel length is 50 mm. For the present experiments, the mass input is a mixture of argon with 1.5% hydrogen, fed through six, optically-triggered fast puff valves, connected by a common reservoir to a plurality of choked orifices in the boron-nitride backplate. The fast puff valves have a risetime of approximately 4 ms to 90% of peak flow. The total input mass flow rate for both configurations in these experiments is 6×10^{-3} kg/s.

The discharge is powered by a 400 kJ capacitor bank connected as an LC-ladder transmission line. At an initial voltage of 18 kV, approximately 45 kA can be delivered to the experiment, with a pulse-width (FWHM) of 0.88 ms; a simple change in connection can provide 90 kA for 0.44 ms. Voltage and current measurements are recorded with digital data acquisition equipment, and analyzed using a dedicated data processing computer in a screened-enclosure adjacent to the experimental area.

Arcjet Operating Characteristics

Typical records of discharge current and terminal voltage (uncorrected for initial and final inductive transients) are displayed in Figs 4a and 4b, for an initial capacitor voltage of 8 kV, and a mass flow rate of 6×10^{-3} kg/s. Quasi-steady operation, as indicated by these measurements, is obtained after about 0.15 ms, and persists for about 0.55 ms, with a discharge current plateau of approximately 21 kA, and a terminal voltage of 48 v. The terminal voltage is monitored using a 1000:1 voltage (divider) probe, connected to the screen room by means of an optical data link. The high frequency oscillations on the terminal voltage are primarily a consequence of the optical data link receiver, and do not necessarily represent voltage fluctuations at the arcjet.

Spectroscopic System

The input power to the arcjet, based on the terminal electrical measurements, is about 1 Mw, which is similar to high power, quasi-steady MPD arcjet operation

studied by other groups for many years^{4,8,12,14}. Based on such studies, it is reasonable to expect a priori that plasma flow speeds on the order of 10^4 m/s will exist within the present arcjets. Such speeds would provide Doppler shifts (and/or widths) of $u/c \sim 3 \times 10^{-5}$, corresponding to 0.014 nm for the Ar II line at 434.8 nm. For sufficient dispersion by a spectrograph, in combination with electronic amplification of the resulting reduced light intensity, non-intrusive measurement of heavy-particle speeds should be possible. Furthermore, entire sections of the arcjet flow field could be sampled on a single shot by employing a two-dimensional detector array.

For such spectroscopic analysis, a digital spectral and spatial data acquisition system has been developed at the RDA Washington Research Laboratory in a cooperative program with a group under Martinez-Sanchez at the Massachusetts Institute of Technology¹⁴. The system, displayed schematically in Fig 1, comprises a 1.2 meter, f/11.5 spectrograph with an EG&G/PARC silicon intensified optical multichannel analyzer (OMA-SIT camera). The OMA-SIT is a two-dimensional (500 x 500) sensor array that can be gated on and off with a pulsewidth down to 40 ns. The spectroscopic system with input optics is mounted on an optical bench adjacent to the thruster and vacuum tank.

In order to observe the flow within the MPD thrust chamber, a set of four slits, 1.4 mm wide, were machined in the outer conductor, symmetrically on a circle in a plane normal to the thruster axis, 22.7 mm from the chamber side of the boron-nitride insulator. By aligning the spectrograph slit perpendicular to the chamber axis of symmetry, simultaneous chordal views can be sampled (vertically) by the sensor array, while the light accumulated along any chordal view is dispersed spectrally (in the horizontal direction). Software then allows the two-dimensional array of light intensity values measured by the sensors to be displayed and manipulated as a function of wavelength and position of the chordal view.

The spectral and spatial output from the camera is processed by an IBM System 9000 laboratory computer for immediate background subtraction and signal averaging. Data acquisition comprises 62.5 kbytes of wavelength/position/intensity values. Software allows correction for systematic errors and noise, prior to attempting to analyze spectral characteristics, such as line shape. The present data collection configuration provides a wavelength resolution of 0.00113 nm/pixel in 3rd order at 434.8 nm, with a spatial resolution at the experiment of 0.25 mm/pixel.

EXPERIMENTAL RESULTS

Inter-Electrode Current Distribution

Magnetic probes (pick-up coils integrating the local rate of change of magnetic field) are inserted in the MPD thrust chamber to delineate the discharge structure. Two magnetic probes at different positions are used simultaneously in order to provide a general correlation of measurements while mapping the current distribution over a large number of shots. Both probes use 1.2 mm (effective) diam coils, encased in 3mm diam Pyrex tubes. The probes are mounted on an externally-controlled, xy-translator that provides a positioning accuracy of ± 0.2 mm. Current contours developed over repeated test firings are displayed for the two arcjet configurations in Figs 2a and 3a, respectively. Note that in the case of mass injection only at mid-radius, there appears to be a persistent inflection in the current contours at mid-radius. Such inflection is not apparent in the second configuration, in which half the mass flow is introduced near the cathode base, and a more open transition to the thrust chamber is provided from the orifices at mid-radius. Also, on average, the current streamlines near the cathode are less axially directed in the case of mass injection at the cathode base. Furthermore, the discharge current flows almost entirely within the thrust chamber with mass injection only at mid-radius, while a significant fraction of the discharge extends beyond the chamber exit plane for the second injector arrangement. It is useful to keep in mind that these two arcjets are operating with the same terminal values of current, input mass flow, and voltage.

Initial Spectroscopic Studies

The first set of spectroscopic studies were performed under the assumption that the flow within the thrust chamber is essentially axial. If this is true everywhere along a chordal view, then standard Abel inversion techniques may be applied to obtain the heavy-particle temperature as a function of radius from spectral data recorded as a function of chordal position. The Abel inversion technique (developed by Keefer, et al) employed in the present experiments utilizes a Fourier transform method^{16,17}, and is effective with noisy data.

Time-integrated line profile measurements are made through the slit in the anode for the case of mid-radius-only injection. Both the Ar II 434.8 nm line and the 696.28 nm line of H_{α} are analyzed in detail. With the system resolution, 94 radial data points are taken per discharge. The Ar II emission is recorded with the spectrograph in second order. The system resolution was 0.002216 nm, with a measured instrument profile that

was Gaussian with a FWHM of 0.01262 nm (± 0.00045 nm). The observed signal, which is an integral along the chord of observation, is spatially filtered, and also filtered with respect to wavelength (with a low frequency bandpass whose cutoff frequencies are determined by the allowable spectral frequencies from the instrument profile). The signal is then Abel-inverted at each observed wavelength to obtain the emission coefficient of the plasma as a function of radius. The resulting line emission profile at each radius is least-squares fitted with a Gaussian distribution in order to determine the heavy-particle temperature as a function of radius. Figure 5 shows the relative intensity of the (integrated) Ar II line as a function of radius, based on Abel inversion of chordal data. The line profile (at a position 13.6 mm from the cathode) is displayed in Fig 6, along with a fit to a Gaussian profile.

The same process of filtering the raw data, and then Abel inverting to obtain the emission as a function of wavelength and radius is applied to the H_{α} line at 696.28 nm. The emission profile is expected to be a combination of Gaussian and Lorentzian profiles (Voigt profile). A deconvolution technique using inverse Fourier transforms is employed to separate these two component profiles^{18,19}. Within 10 mm of the anode surface, fitting the Lorentzian component of the line profile in terms of Stark broadening²⁰⁻²² indicates electron densities of $1.5 - 4 \times 10^{15} \text{ cm}^{-3}$. For radial positions more than 10 mm from the anode surface, no Lorentzian component could be extracted, suggesting that the electron densities are less than $\sim 10^{15} \text{ cm}^{-3}$, at the particular axial station examined here.

The Gaussian component of the deconvolved hydrogen emission profile indicates a heavy-particle temperature of ~ 0.5 eV, whereas a fit to the Ar II profile at the same position suggests an argon ion temperature of 13.6 eV. For particle densities of about 10^{15} cm^{-3} , and a temperature of the lighter hydrogen ("field") particle of 1 eV, the energy equipartition time²³ based on classical Coulomb collisions is less than 50 ns. At a speed of 10^4 m/s, hydrogen and argon ions would have the opportunity to achieve the same temperature in distances of less than 0.5 mm, which is less than the streamwise size of the emitting region sampled. The substantial disagreement between the two estimates of heavy-particle temperature suggests that a significant discrepancy might exist in applying conventional spectroscopic analysis to the flow within the MPD thruster (and possibly to other similar situations as well). In particular, the initial simplification of strictly axial flow can be inappropriate even though the solid boundaries channeling the flow are straight and parallel to the thruster axis.

New Technique for Measurement of Speed, Turbulence, and Temperature

The distribution of light intensity accumulated along chordal views of an axisymmetric, optically-thin radiator is usually converted to an emission intensity per unit volume as a function of cylindrical radius by means of the Abel inversion. It is necessary in performing this inversion that, for each volume element sampled along the chord, the radiation is emitted isotropically (at least in the plane normal to the cylindrical axis) in each wavelength of interest. This condition is satisfied for radiators in random thermal motion, and also for turbulent motion of the radiating fluid, to the extent that, for each radiating element, there is zero net velocity along the chordal view, averaged over both the spatial and time scales of the measurement. If there is a net chordal component of flow velocity, in space and/or time, then the standard application of the Abel inversion can lead to erroneous results. Chordal views across an axisymmetric flow in which net local radial velocities are significant compared to the random thermal (or local turbulent) speed of the radiators can include Doppler shifts symmetrically about the natural line center. These shifts might then be incorrectly included as Doppler broadening in the course of fitting a Gaussian profile to the line shape.

Figure 7 schematically depicts the components of the line shapes obtained by two different chordal views of radiating elements at the same radial position in an axisymmetric flow. If there are velocity components along the chordal view due to a symmetrical, radial motion of the fluid at speed v_r , then the volume emission coefficient as a function of chordal position (defined by the angle θ) will include additions and subtractions to the random speed (due to thermal and local turbulent motions):

$$\epsilon(r, \lambda) = \frac{\epsilon(r)}{\sqrt{\pi} \Delta \lambda_D} \exp \left[- \left(\frac{\Delta \lambda \pm \lambda_0 \frac{v_r \sin \theta}{c}}{\Delta \lambda_D} \right)^2 \right]$$

where $\epsilon(r)$ is the emission coefficient integrated over all wavelengths, $\Delta \lambda$ is the wavelength relative to the natural line center λ_0 , and the Doppler width, $\Delta \lambda_D$, is given in terms of a mean turbulent speed $\langle v \rangle$, and a mean thermal speed based on the local temperature T , and the molecular mass of the radiator, m ^{22,24,25}:

$$\Delta \lambda_D^2 = \left(\frac{\lambda_0}{c} \langle v \rangle \right)^2 + \left(\frac{\lambda_0}{c} \sqrt{\frac{2kT}{m}} \right)^2$$

The total emission coefficient as a function of radius is found by first integrating the intensity over the line shape at each chordal view, to obtain a quantity that is independent of the angle between the chord and the radial flow, and then Abel inverting this axisymmetric quantity.

For a particular radiating specie, the effects of random motion are separated from the Doppler shifts due to net radial velocity by the following procedure. The axisymmetric radiating flow is considered as a set of coaxial shells, each characterized by a net radial flow speed, a random speed, and an emission coefficient. At the outermost shell, the line shape is essentially due to Doppler broadening, (since the flow velocity has a negligible component with respect to the chordal view), so the random speed for this shell can be computed. The chordal view of the next inner shell has contributions due to the outer shell, with symmetric Doppler shifts associated with the radial speed of this shell, and a contribution due to the inner shell that is only Doppler broadened, (since the chordal view is again at grazing incidence). A two-parameter, least-squares fit is made to the measurement at this chord, using two symmetrically displaced Gaussians of unknown shift, but known amplitude and width (based on the previous shell measurement), and an unshifted Gaussian of known amplitude, but unknown width. The resulting best-fit parameter values provide the net radial speed of the previous shell, and the random speed of the present shell. With these values, the procedure can then be continued to the inner shells, at each stage obtaining the random speed of a particular shell, and the radial speed of the previous one.

Figure 8 displays the distribution of radial speed vs radial distance from the cathode, based on the above procedure, for the case of mid-radius-only injection. The radial speed appears to decrease as the axially-aligned electrode boundaries are approached, as expected, but a maximum radial speed comparable to anticipated axial speeds is also indicated within the straight-walled flow channel. By applying the unfolding procedure both to argon and hydrogen lines, and assuming that these two species have the same temperature and fluid speeds (directed and turbulent), it is possible to differentiate between thermal and turbulent contributions to the random speed. In Fig 9, the resulting distributions of heavy-particle temperature, and (in-plane) turbulent speed, averaged over the duration of the quasi-steady flow, are shown vs radial distance from the cathode. Temperature and turbulence are both seen to increase from anode to cathode, at least at the particular axial station of the measurement (22.7 mm from

the insulator), with the turbulent speed achieving its highest value adjacent to the cathode surface.

The corresponding distributions of radial speed, temperature, and turbulent speed for the second arcjet configuration (50% mass flow at the cathode base), displayed in Figs 10 and 11, have significantly lower amplitudes at most radial locations, suggesting that this mass flow arrangement provides more uniform axial direction of the flow, (at least at this axial position). The heavy-particle temperature appears to increase rapidly toward the anode vs the cathode in this configuration, however, so further variation of mass injection design might be usefully explored. (Observation of the reduced line width is accomplished by operating the spectrograph in third order, providing a wavelength resolution of 0.00113 nm/pixel, and by reducing the measured instrument profile FWHM to 0.0043 nm (+/-)0.00012 nm.)

MHD CODE RESULTS

In addition to the experimental effort, a short series of numerical code simulations of the MPD thrust chamber flow have been performed to provide some initial indication of flow field behavior, and also to evaluate the ability of the existing MACH2 computer code¹⁵ to handle MPD arcjet problems. The code has been developed over the last several years, primarily to assist in the analysis and design of very high power, pulsed coaxial plasma guns²⁶, and, more recently, coaxial plasma accelerators involving applied axial magnetic fields, (in particular, compact toroid plasma/magnetic field systems). MACH2 is presently a two-dimensional (plus axisymmetric rotation), single-fluid MHD code. It is based on an adaptive Lagrangian-Eulerian formulation, and is readily configured for complex (axisymmetric) channel boundaries. The equation of state options presently available are both single-temperature, (perfect gas, or tabular data for a wide variety of materials). Thermal and magnetic diffusion, radiative emission, and Hall effect are all included. For low density, high current discharges, anomalous electrical resistivity is modeled based on micro-instability theory.

Figures 12 - 15 display results from the MACH2 code for conditions resembling those of the experimental tests, in terms of electrode dimensions, total current, and total mass flow rate. For simplicity in the limited effort available, the mass flow is injected uniformly through the insulator backplate, and the cathode is truncated sharply at the anode exit plane. The current contours shown in Fig 12 resemble those for the first arcjet (mid-radius-only injection) in regard to the retention of current flow within the thrust chamber. With uniform mass injection, there is no indication in the

code results of an inflection of the current streamlines at mid-radius.

At an axial position corresponding to the measurement station of the spectroscopic studies, the single-temperature code computes a temperature that rises from about 1.4 to 2.8 eV in traversing from the anode to the cathode. While these values are significantly higher than estimates from spectroscopic study of the first arcjet configuration, the increase in temperature toward the cathode is similar. A decrease in particle density, with density values in the range of 10^{15} cm^{-3} , radially inward from the anode is also implied by both the code and the earlier Stark broadening data. The velocity vectors shown in Fig 15 have maximum computed values of $3.5 \times 10^4 \text{ m/s}$, for very low density flow in the thruster exhaust. Within the thrust chamber itself, maximum total speeds are about $2.4 \times 10^4 \text{ m/s}$, in the low density flow approximately one-third of the inter-electrode gap from the cathode surface. The calculated flow field within the thrust chamber has the appearance of plasma expanding from a relatively high pressure region near the cathode base, while constrained to curve axially downstream under the influence of the electromagnetic forces in the discharge. At the measurement station, this flow field would exhibit a maximum radial speed at about 6.4 mm from the cathode surface, in good agreement with the experimentally-derived distribution. (The code calculations, however, indicate a radial speed at this position of about $5 \times 10^3 \text{ m/s}$, which is less than half of the spectroscopic result.) Close comparison of computational and experimental results would require more extensive modeling, and measurements at additional axial stations, in order to discern differences that are due only to variances in exact geometry or location. A moderate amount of further code development would also be useful to allow for nonequilibrium conditions, (e.g., electron vs heavy-particle temperature), and electrode boundary effects.

CONCLUDING REMARKS

The present experimental and computational efforts indicate that significant variations of flow dynamics within an MPD arcjet thrust chamber are available simply by altering the mass flow injection arrangement, with the terminal properties of the arcjet held fixed. It is expected that variation of current or mass flow delivered to an arcjet with a fixed injector arrangement and channel geometry will, likewise, substantially change the internal flow. Even apart from uncertainties in behavior due to changes in electrode operation with flow conditions, the basic flow within the MPD thrust chamber may not yet be well understood, (let alone controlled). The present code results, for example,

suggest a rather unconventional picture of the MPD thruster flow, in which the so-called "pumping" mode, normally associated with the formation of a plasma jet off the cathode tip, is actually established along the length of the cathode surface. (This was previously noted in Ref. 8). The high pressure usually thought to be exerted at the cathode tip is instead supported by the axial electromagnetic force ("blowing" mode) and kinetic pressure gradient near the cathode base. (It is almost certainly true that not every MPD arcjet will operate in this fashion, under all conditions of current and mass flow rate.)

Since thruster performance, in terms of lifetime and efficiency, should be expected to vary significantly with variations in the flow field, and interactions of the flow with boundaries, evaluation of the potential of MPD arcjets for space missions cannot be reasonably based on empirical surveys of terminal properties for a limited number of devices. Instead, computational tools, validated by close comparison with experimentally-determined flow fields in at least a few representative thruster arrangements, must be employed to select and optimize candidates for further experimental development. The present paper demonstrates both experimental and computational techniques that can be used to accomplish a consistent and valid examination of MPD arcjet behavior, but much more work remains to be done.

ACKNOWLEDGEMENTS

This work was supported by the Air Force Office of Scientific Research, Directorate of Aerospace Sciences. The earlier cooperative research effort with the MIT group under Prof. M. Martinez-Sanchez, also funded by AFOSR, was of great benefit. The advice and assistance on electronic problems of Dr. S. Seiler of RDA is gratefully noted.

REFERENCES

- 1 Ducati, A., et al, AIAA Journal, Vol. 2, 1964, p. 1452.
- 2 Patrick, R.M. and Schneiderman, A.M., AIAA Journal, Vol. 4, 1966, p. 283.
- 3 Fradkin, D.B., et al, AIAA Journal, Vol. 8, 1970.
- 4 Clark, K.E. and Jahn, R.G., AIAA Journal, Vol. 8, 1970.
- 5 Michels, C.J. and Sigman, D.R., AIAA Journal, Vol. 9, 1971.
- 6 Malliaris, A.C., et al, AIAA Journal, Vol. 10, 1972, p. 121.

- 7 Jahn, R.G., Physics of Electric Propulsion, McGraw-Hill, NY, 1968, Chapter 8.
- 8 Turchi, P.J. and Jahn, R.G., AIAA Journal, Vol. 9, 1971, p. 1372.
- 9 Jahn, R.G., et al, AIAA Journal, Vol. 9, 1971, p. 167.
- 10 Kribel, R., et al, AIAA Journal, Vol. 9, 1971.
- 11 Oberth, R.C. and Jahn, R.G., AIAA Journal, Vol. 10, 1972.
- 12 Bruckner, A.P. and Jahn, R.G., AIAA Journal, Vol. 12, 1974, p. 1198.
- 13 Aeschliman, D.P. and Evans, D.L., J. Quant. Spectroscopy and Rad. Transfer, Vol. 16, 1976, p. 191.
- 14 Heimerdinger, D.J., et al, "Effect of Axial Variation of Electrode Spacing on MPD Arcjet Behavior", 19th International Electric Propulsion Conference, Colorado Springs, CO, May 11-13, 1987.
- 15 Buff, J., et al, IEEE Transactions on Plasma Science, Vol. PS-15, 1987, p. 766.
- 16 Keefer, D.R., et al, J. Quant. Spectroscopy and Rad. Transfer, Vol. 39, 1988, p. 367.
- 17 Smith, L.M., IEEE Transactions on Information Theory, Vol. 34, 1988, p. 158.
- 18 Harris, J.L., Sr., J. Optical Soc. of America, Vol. 56, 1966, p. 569.
- 19 Helstrom, C.W., J. Optical Soc. of America, Vol. 57, 1967, p. 569.
- 20 Wiese, W.L., in Plasma Diagnostic Techniques, eds. R.H. Huddleston and S.L. Leonard, Academic Press, NY, 1965. Chapter 6.
- 21 Traving, G., in Plasma Diagnostics, ed. W. Lochte-Holtgreven, North-Holland Publishing, Amsterdam, 1968. Chapter 2.
- 22 Griem, H.R., Plasma Spectroscopy, McGraw-Hill, NY, 1964. Chapter 4.
- 23 Spitzer, L., Jr., Physics of Fully Ionized Gases, Interscience, NY, 1962. Chapter 5.
- 24 Zhi, G. and Qian, J., Applied Optics, Vol. 26, 1987, p. 1956.
- 25 Hinze, J.O., Turbulence, McGraw-Hill, NY, 1975.
- 26 Turchi, P.J., et al, IEEE Transactions on Plasma Science, Vol. PS-15, 1987, p. 747.

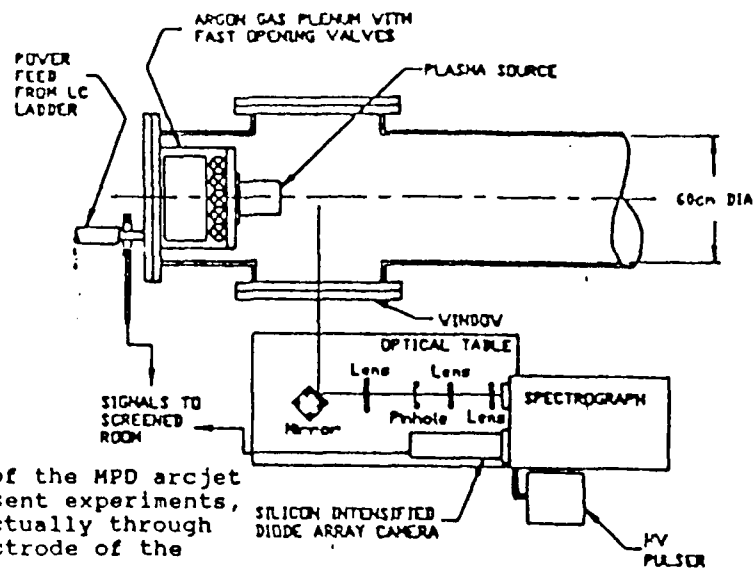


Fig. 1 : Basic layout of the MPD arcjet experiment. In the present experiments, the line of sight is actually through slits in the outer electrode of the thruster.

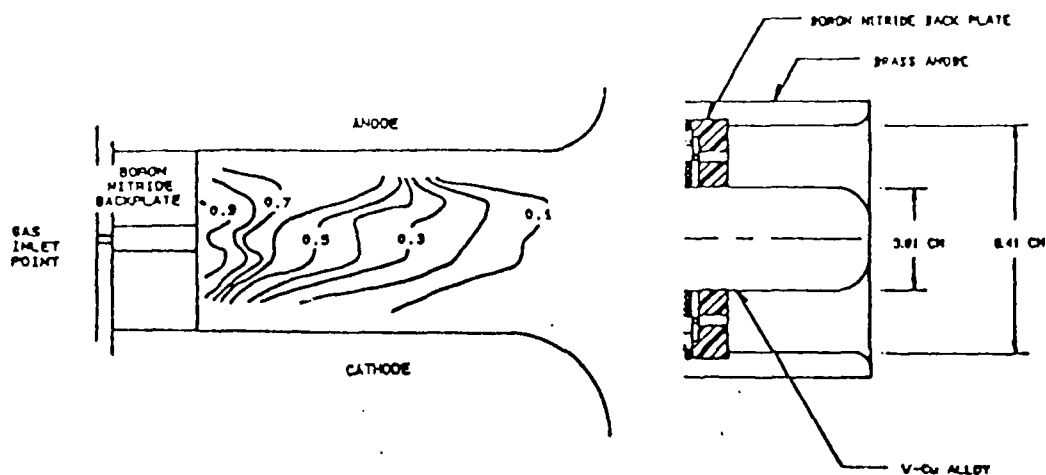


Fig. 2 : a) Current contours for the case of mass injection only at mid-radius; b) schematic diagram of MPD arcjet with mid-radius only injector arrangement.

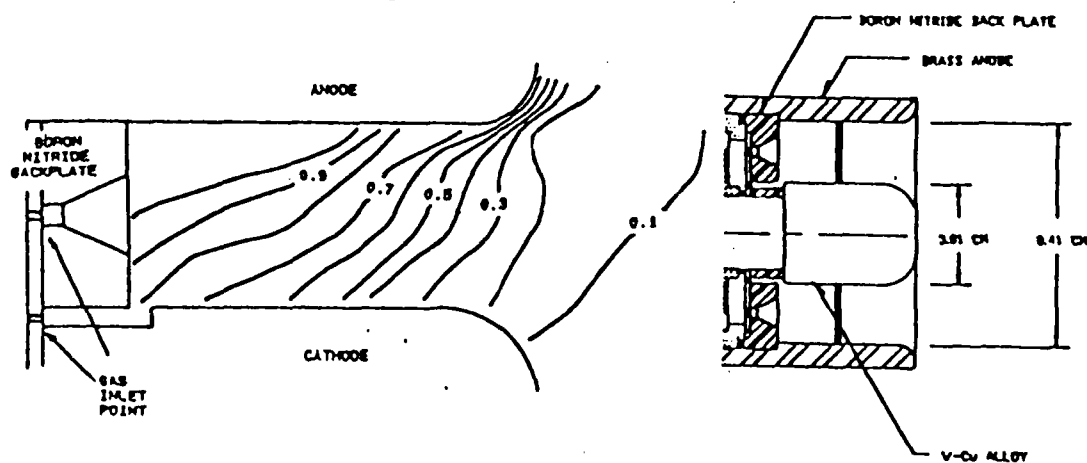


Fig. 3 : a) Current contours for the case of 50% mass injection near the cathode base, and 50% at mid-radius; b) schematic diagram of MPD arcjet with mass injection at cathode base, and modified mid-radius injector geometry.

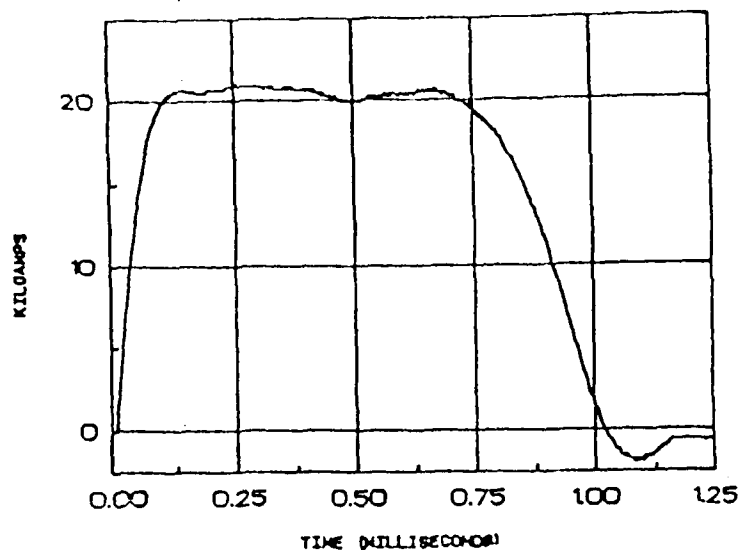


Fig. 4 : a) arcjet current vs time for an initial voltage of 8 kV on the LC-ladder capacitor bank; b) terminal voltage at the arcjet (not corrected for inductive voltage transients).

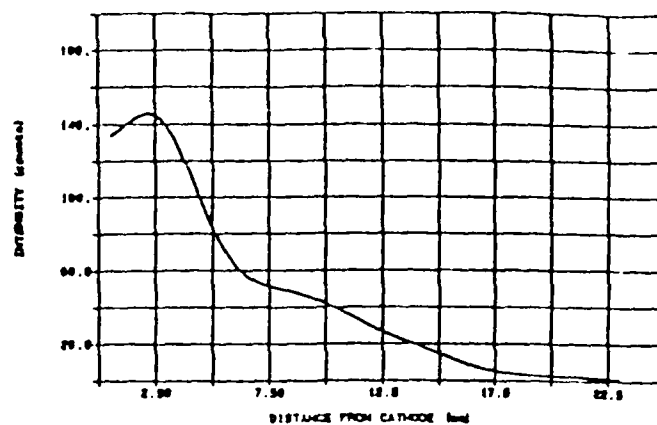


Fig. 5 : Relative intensity of the (integrated) Ar II line as a function of radius.

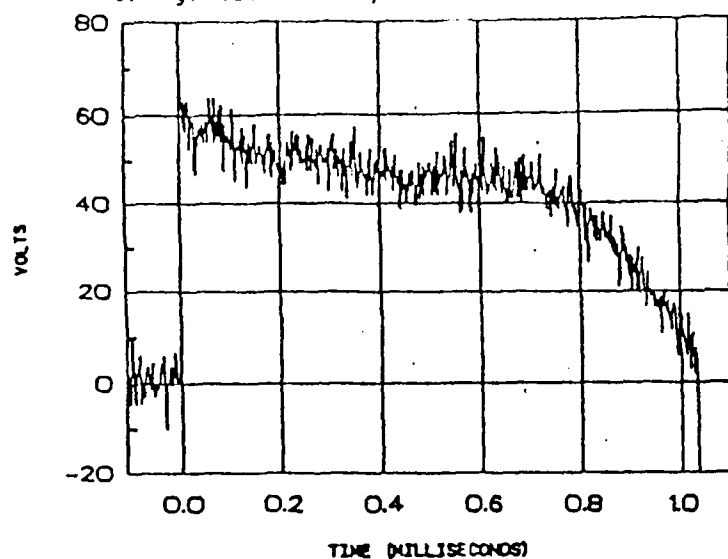


Fig. 6 : Profile of Ar II line (434.8 nm) at 13.6 mm from the cathode surface. Least-squares fit to a Gaussian distribution is also shown.

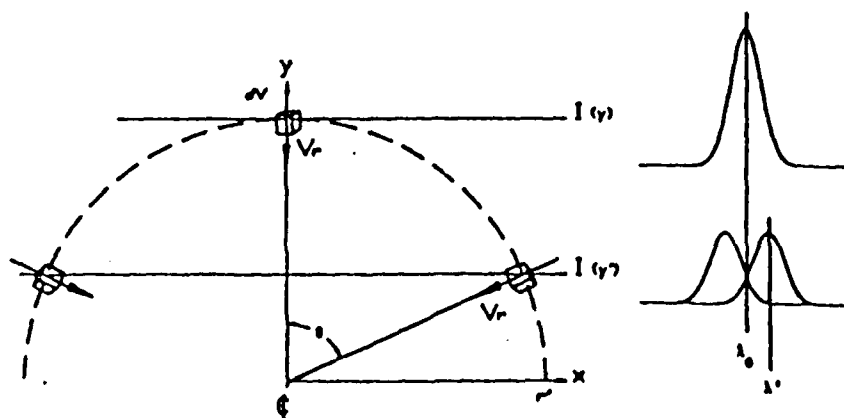


Fig. 7 : Schematic representation of line profiles obtained by sampling the same cylindrical shell at different chordal views for non-zero radial speed.

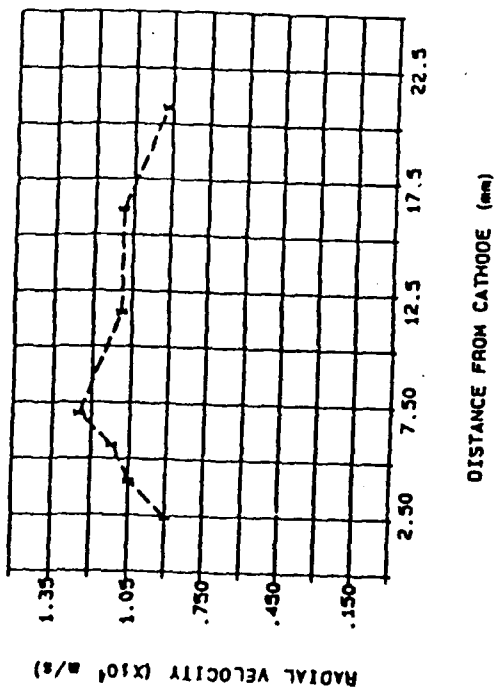


Fig. 8 : Distribution of radial speed vs radial position for case of mid-radius-only injection.

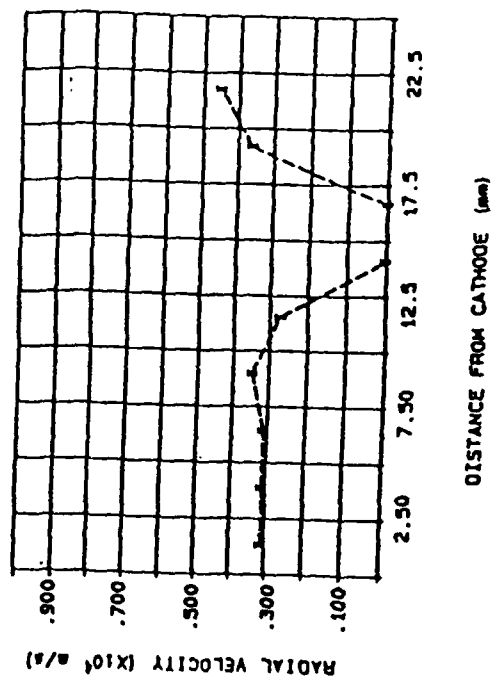


Fig. 10 : Distribution of radial speed vs radial position for case of 50% mass injection near the cathode base.

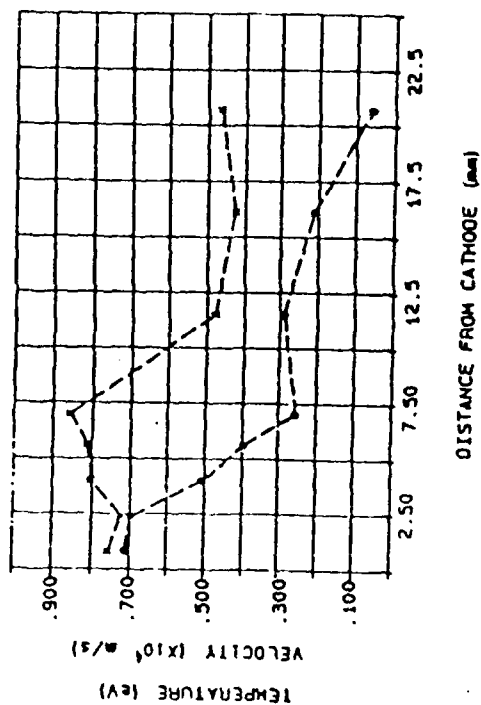


Fig. 9 : Distributions of temperature (upper curve) and turbulent speed (lower curve) for case of mid-radius-only injection, based on both argon and hydrogen emission analysis.

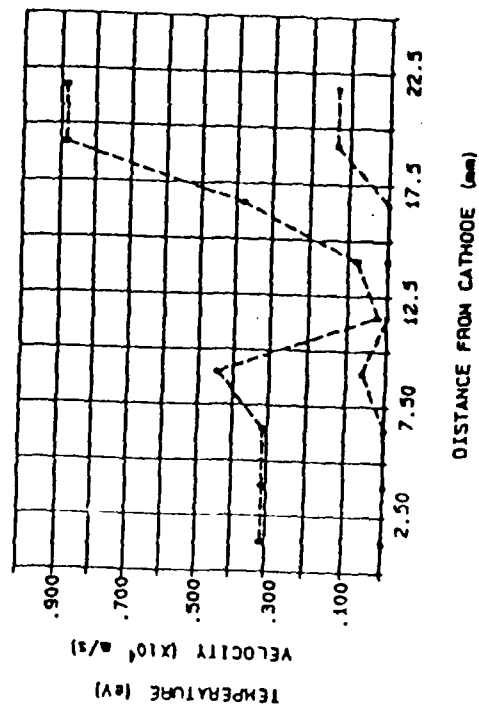


Fig. 11 : Distributions of temperature (upper curve) and turbulent speed (lower curve) for case of 50% mass injection near the cathode base.

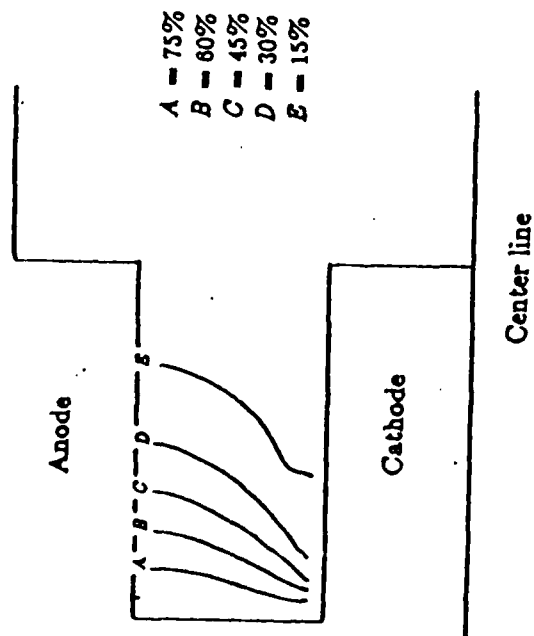


Fig. 12 : Current contours calculated by MACH2 computer code for case of uniform mass injection (at 6 g/s) through insulator backplate. Total current is 21 kA.

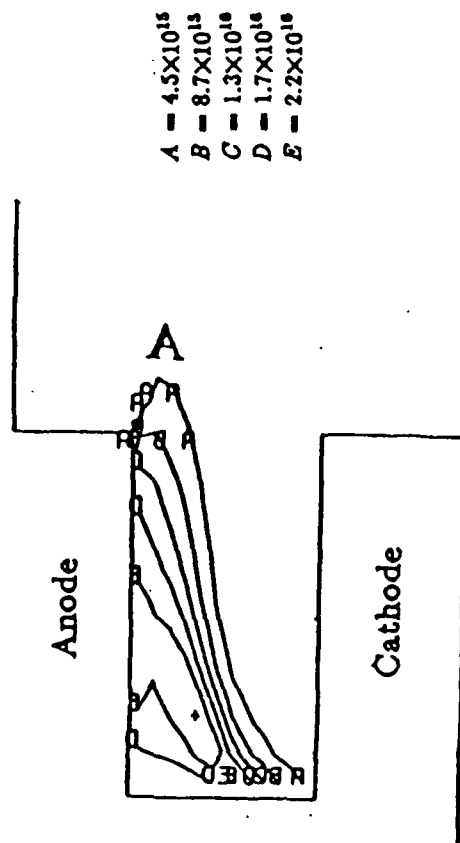


Fig. 14 : Constant number density contours in units of $[\text{cm}^{-3}]$ calculated by MACH2 computer for case of Fig. 12.

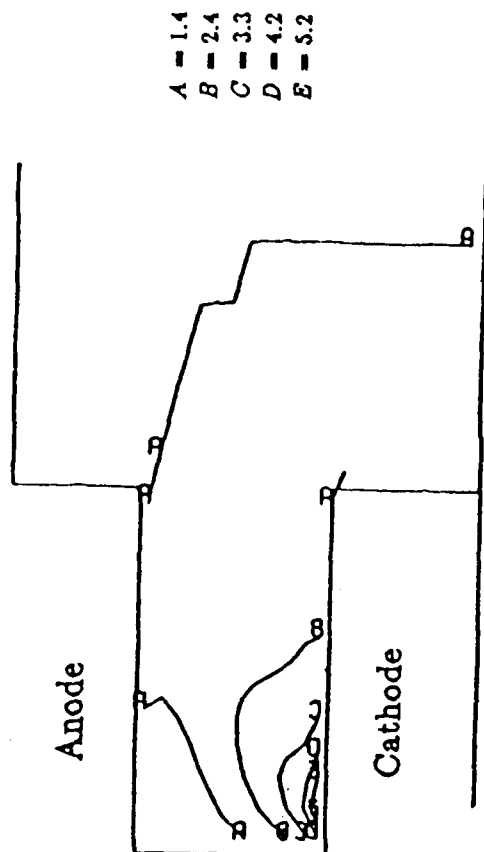


Fig. 13 : Constant temperature contours in units of $[\text{eV}]$ calculated by MACH2 computer code for case of Fig. 12.

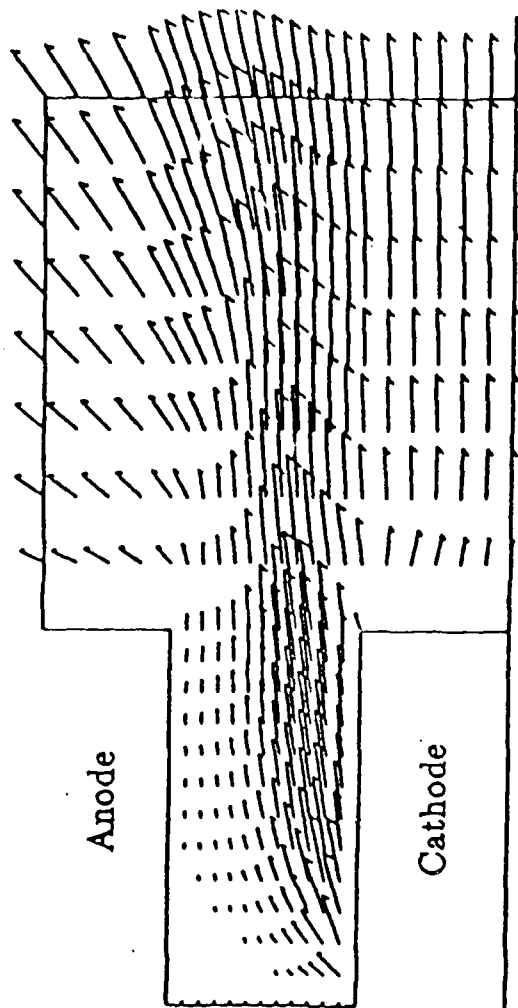


Fig. 15 : Distribution of flow velocity calculated by MACH2 computer code for case of Fig. 12. Magnitude of longest vector (well downstream of cathode corner) is $3.5 \times 10^4 \text{ m/s}$.